



1 Observations of particle number size distributions and new 2 particle formation in six Indian locations

3

4 Mathew Sebastian¹, Sobhan Kumar Kompalli², Anil Kumar³, Sandhya Jose^{4,5}, S. Suresh Babu²,
5 Govindan Pandithurai³, Sachidanand Singh^{4,5}, Rakesh K. Hooda⁶, Vijay K. Soni⁷, Jeffrey R.
6 Pierce⁸, Ville Vakkari^{6,9}, Eija Asmi⁶, Daniel M. Westervelt^{10,11}, Antti-P. Hyvärinen⁶, and Vijay P.
7 Kanawade^{1,*}

8

9 ¹Centre for Earth, Ocean and Atmospheric Sciences, University of Hyderabad, Hyderabad, India

10 ²Space Physics Laboratory, Vikram Sarabhai Space Centre, Thiruvananthapuram, India

11 ³Indian Institute of Tropical Meteorology, Ministry of Earth Sciences, Pune, India

12 ⁴CSIR-National Physical Laboratory, Dr. K.S. Krishnan Road, New Delhi, India

13 ⁵Academy of Scientific and Innovative Research (AcSIR), Ghaziabad-201002, India

14 ⁶Finnish Meteorological Institute, Erik Palmenin Aukio 1, Helsinki, Finland

15 ⁷India Meteorological Department, Ministry of Earth Sciences, New Delhi, India

16 ⁸Department of Atmospheric Science, Colorado State University, Fort Collins, CO, USA

17 ⁹Atmospheric Chemistry Research Group, Chemical Resource Beneficiation, North-West University, Potchefstroom,
18 South Africa

19 ¹⁰Lamont-Doherty Earth Observatory of Columbia University, New York, USA

20 ¹¹NASA Goddard Institute for Space Studies, New York, NY, USA

21

22 Correspondence to: Vijay P. Kanawade (vijaykanawade03@yahoo.co.in)

23

24 **Abstract.** Atmospheric new particle formation (NPF) is a crucial process driving aerosol number
25 concentrations in the atmosphere; it can significantly impact the evolution of atmospheric aerosol
26 and cloud processes. This study analyses at least one year of asynchronous particle number size
27 distributions at six different locations in India. We also analyze the frequency of NPF and its
28 contribution to cloud condensation nuclei (CCN) concentrations. We found that the NPF frequency
29 has a considerable seasonal variability. At the measurement sites analyzed in this study, NPF
30 frequently occurs in March-May (pre-monsoon, about 21% of the days) and is the least common
31 in October-November (post-monsoon, about 7% of the days). Considering the NPF events in all
32 locations, the particle formation rate (J_{NUC}) varied by more than an order of magnitude (0.01 - 0.6



33 $\text{cm}^{-3} \text{s}^{-1}$) and the growth rate (GR_{NUC}) by about three orders of magnitude ($0.2 - 17.2 \text{ nm h}^{-1}$). We
34 found that J_{NUC} was higher by nearly an order of magnitude during NPF events in urban areas than
35 mountain sites. GR_{NUC} did not show a systematic difference. Our results showed that NPF events
36 could significantly modulate the shape of particle number size distributions and CCN
37 concentrations in India. The contribution of a given NPF event to CCN concentrations was the
38 highest in urban locations ($4.3 \times 10^3 \text{ cm}^{-3}$ per event and $1.2 \times 10^3 \text{ cm}^{-3}$ per event for 50 nm and 100
39 nm, respectively) as compared to mountain-background sites ($2.7 \times 10^3 \text{ cm}^{-3}$ per event and 1.0×10^3
40 cm^{-3} per event). To better understand atmospheric NPF and its contribution to CCN concentrations,
41 we would need long-term observational data from various diverse environments in India, aided
42 with regional model simulations to help interpret field observations.

43

44 **Keywords:** new particle formation, particle number size distribution, Aitken mode, accumulation
45 mode, cloud condensation nuclei

46

47 **1 Introduction**

48 Cooling by atmospheric aerosols offset a significant fraction of the radiative forcing of the
49 greenhouse gases (Paasonen et al., 2013) directly by scattering and absorbing solar radiation and
50 indirectly by altering cloud microphysical properties via activation of cloud condensation nuclei
51 (CCN) (Rosenfeld et al., 2014; Sarangi et al., 2018). New particle formation (NPF), as a result of
52 the gas-to-particle conversion, is the largest source of the aerosol number to the terrestrial
53 atmosphere (Kulmala et al., 2007; Zhang et al., 2012). While nucleated particles from NPF are
54 initially very small molecular clusters (1-2 nm; Kerminen et al., 2012), these molecular clusters
55 can grow to large sizes within a few hours to a few days and ultimately reach CCN-active sizes
56 ($>50\text{-}100 \text{ nm}$) (Pierce and Adams, 2007; Westervelt et al., 2013). Thus, CCN forms the direct
57 microphysical link between aerosols and clouds and plays a vital role in the hydrological cycle and
58 climate.

59 In India, several intensive field campaigns such as the Indian Ocean Experiment
60 (INDOEX) (Ramanathan et al., 2001), Indian Space Research Organization (ISRO)-Geosphere-
61 Biosphere Programme (GBP)- Land campaign II (Tripathi et al., 2006; Tare et al., 2006), and
62 Integrated Campaign for Aerosols, gases, and Radiation Budget (ICARB) (Moorthy et al., 2008;
63 Nair et al., 2020; Kompalli et al., 2020) measured sub-micron particle number size distributions



64 (PNSDs). There are also short- and long-term field observations of sub-micron PNSDs in a variety
65 of diverse locations in India (Hyvärinen et al., 2010; Kanawade et al., 2014a; Shika et al., 2020;
66 Tripathi et al., 1988; Kompula et al., 2009; Singh et al., 2004; Moorthy et al., 2011; Babu et al.,
67 2016; Kompalli et al., 2018). But there are sparse studies in India characterizing seasonal variation
68 in PNSDs and number concentrations (Kanawade et al., 2014a; Hyvärinen et al., 2010; Kompula
69 et al., 2009; Hooda et al., 2018; Laj et al., 2020) and atmospheric NPF (Sebastian et al., 2021b;
70 Siingh et al., 2018; Neitola et al., 2011; Moorthy et al., 2011; Kanawade et al., 2014b; Kanawade
71 et al., 2014c; Kanawade et al., 2020a). The characterization of PNSDs is critical because the PNSD
72 is controlled by an evolving balance between NPF, condensation of vapor on pre-existing particles,
73 evaporation of particles, coagulation and sedimentation (Ipcc, 2013). Previous field measurements
74 and modeling studies globally demonstrated a substantial enhancement in CCN number
75 concentrations from nucleation (Yu et al., 2020; Wiedensohler et al., 2009; Sihto et al., 2011; Rose
76 et al., 2017; Tröstl et al., 2016; Kalivitis et al., 2015; Westervelt et al., 2013; Pierce et al., 2012;
77 Pierce et al., 2014; Westervelt et al., 2014; Kerminen et al., 2012; Kerminen et al., 2018; Merikanto
78 et al., 2009; Gordon et al., 2017). For instance, Merikanto et al. (2009) revealed that 45% of the
79 global low-level CCN at 0.2% supersaturation originates from nucleation. Westervelt et al. (2014)
80 also found that nucleation contributes to about half of the boundary layer CCN (at supersaturation
81 of 0.2%), with an estimated uncertainty range of 49 to 78%, which is sensitive to the choice of
82 nucleation scheme. In contrast, Reddington et al. (2011), using the global model GLOMAP against
83 ground-based measurements at 15 European sites, found that CCN-sized particle number
84 concentrations were driven by processes other than nucleation at more than ten sites. They
85 explained that the weakened response of CCN-sized particles to boundary layer nucleation arises
86 from an increase in coagulation and condensation sinks for ultrafine particles, thereby reducing
87 the condensational growth of ultrafine particles to CCN-active sizes (Kuang et al., 2009; Pierce
88 and Adams, 2007). Tröstl et al. (2016) also revealed that only a small fraction of total particles less
89 than 50 nm grew beyond 90 nm (50-100 particles cm⁻³), even on a timescale of several days.
90 Therefore, to better understand atmospheric NPF and its contribution to the boundary layer CCN
91 budget, we need highly-resolved spatiotemporal observational data in diverse environments
92 globally, aided with aerosol model simulations, to help to interpret field observations.

93 Overall, studies pertinent to the impact of NPF on aerosol-cloud interactions are highly
94 sparse in India. The sources of aerosols, and gaseous precursors required for secondary aerosol



95 formation, depict a considerable spatiotemporal heterogeneity over India. Therefore, observational
96 aerosols and precursors data must be synthesized to understand the processes that govern NPF and
97 its contribution to CCN concentrations in different settings of India. The primary objective of this
98 study is to harmonize observational PNSDs data from six diverse locations in India to present
99 analyses of PNSDs, atmospheric NPF, and the contribution of NPF to CCN concentrations.

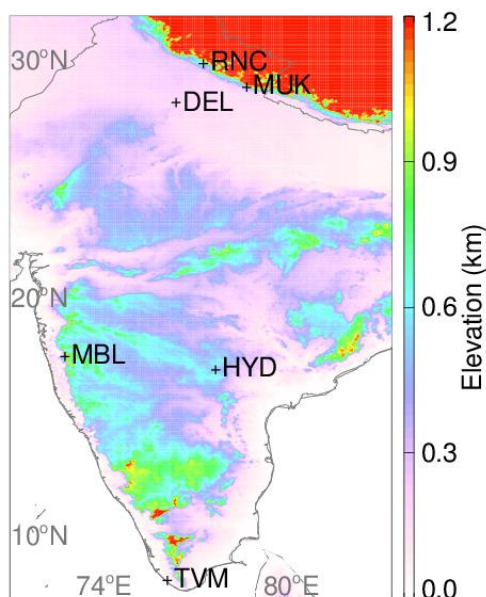
100

101 2 Methods

102 2.1 Observation sites and aerosol sampling instrumentation

103 Figure 1 shows the geographical location of measurement sites on the surface elevation
104 map. Table 1 provides details of measurement sites and particle data analyzed in this study.

105



106

107 **Figure 1.** The geographical location of measurement sites on the surface elevation map.
108 Measurement sites such as Ranichauri (RNC), Mukteshwar (MUK), Mahabaleshwar (MBL),
109 Hyderabad (HYD), Thiruvananthapuram (TVM), and Delhi (DEL) are shown by the plus sign.
110 The global 1-arcsecond (30-m) SRTM digital surface elevation data is obtained from the United
111 States Geological Survey (https://dds.cr.usgs.gov/srtm/version2_1/SRTM30/).



112 **Table 1.** Details of the measurement sites and particle number size distribution measurements
113 analyzed in this study.

Site Name	Site code	Site type	Instrument	Size range (nm)	Time resolution (minutes)	Time Period
Ranichauri	RNC	Mountain background	DMPS	10.1–757	10	12/2016 – 09/2018
Mukteshwar	MUK	Mountain background	DMPS	10.1–757	5	01/2012 – 12/2013
Mahabaleshwar	MBL	Mountain semi-rural	WRAS	5.14–1000	4	03/2015 – 03/2016
Hyderabad	HYD	Urban	SMPS	10.9–514	5	04/2019 – 03/2020
Thiruvananthapuram	TVM	Semi-urban coastal	SMPS	14.6–661.2	5	01/2013 – 01/2014
Delhi	DEL	Urban	WRAS	5.14–1000	5	11/2011 – 01/2013

114 DMPS: Differential Mobility Particle Sizer, WRAS: Wide-Range Aerosol Spectrometer, SMPS:
115 Scanning Mobility Particle Sizer

116

117 Ranichauri observation site (RNC, 30.2° N, 78.25° E; ~1930 m above mean sea level, amsl)
118 is located in Tehri–Garhwal district of Uttarakhand state in the southern slope of the Western
119 Himalaya. The RNC site is situated on an isolated hilltop within the campus of the College of
120 Forestry in the Ranichauri village. The RNC site is a Climate Monitoring station managed by the
121 India Meteorological Department (IMD). It is a mountain background remote observatory
122 (Sebastian et al., 2021b) and located about 70 km to the northeast of Rishikesh city, about 100 km
123 to the northwest of the Srinagar city, and about 100 km to the east of Dehradun. Here, particle
124 number size distributions in the size range from 10 nm to 757 nm (30 size bins) is measured using
125 a differential mobility particle sizer (DMPS, Finnish Meteorological Institute assembled) from
126 December 2016 – September 2018 are used (Sebastian et al., 2021b). The DMPS consisted of a
127 Vienna-type differential mobility analyzer (DMA) that classifies the charged particles according
128 to their electrical mobility and a TSI 3772 condensation particle counter (CPC) that counts
129 particles of the selected mobility. The sample air was drawn inside through a stainless-steel inlet
130 tube of about 2 meters in length and dried to less than 40% relative humidity with a Nafion dryer
131 (Perma Pure model MD-700-48). Diffusion losses in the inlet and inside the DMPS instrument
132 were considered in the data inversion. The inversion method was identical to that presented by
133 Wiedensohler et al. (2012) for the Finnish Meteorological Institute (FMI) DMPS.



134 Mukteshwar observation site (MUK, 29.43° N, 79.62° E, 2180 m amsl) is located in the
135 Nainital district of Uttarakhand state in the southern slope of the Central Himalaya. The
136 Mukteshwar village is situated 3 km to the northeast of the measurement site at a similar altitude
137 with ~800 inhabitants (Census of India, 2011). MUK can be considered a mountain background
138 site, with the annual mean black carbon (BC) concentration of 0.9 $\mu\text{g m}^{-3}$. The town of Almora
139 (1650 m amsl, 34,000 inhabitants) is located at about 16 km to the north, Nainital (1960 m amsl,
140 41000 inhabitants) is located at about 25 km to the southwest, and the city of Haldwani (424 m
141 amsl, 150,000 inhabitants) is located at about 32 km to the southwest to MUK. Delhi, the major
142 metropolitan city (215 m amsl, 16.8 million inhabitants), is located approximately 250 km to the
143 southwest. Systematic measurements of aerosol properties have been conducted at MUK since
144 2005 in Indo-Finnish cooperation with the Finnish Meteorological Institute (Hooda et al., 2018
145 and references therein). Here, we used only two years (January 2012 to December 2013) of
146 measurements of particle number size distributions in the size range of 10 nm to 757 nm (30 size
147 bins). The air sampling procedure was similar to that of the RNC observation site.

148 Delhi observation site (DEL, 28.64° N, 77.17° E, 215 m amsl) is located at CSIR-National
149 Physical Laboratory (NPL). Delhi, India's national capital and largest metropolitan city in South
150 Asia, is located in the northwestern Indo Gangetic Plain (IGP) in northern India. Delhi city has a
151 population of 16.8 million, with a population density of 11,320 km^{-2} (Census of India, 2011). The
152 Great Indian Desert (Thar Desert) of Rajasthan state is located to the southwest, hot central plains
153 to the south, and hilly regions to the north and east of Delhi. Long-range transported air masses
154 often influence Delhi's air quality from the northwest (agricultural residue burning from Punjab
155 and Haryana in October-November) and southwest (dust storms from Thar and Arabian Peninsula
156 in April-June) (Kanawade et al., 2020b; Srivastava et al., 2014). Wide Range Aerosol
157 Spectrometer (WRAS, manufactured by GRIMM, Germany), installed on the second floor of the
158 NPL main building, was used to measure particle number size distributions. WRAS consists of a
159 Scanning Mobility Particle Sizer (SMPS) and an Environmental Dust Monitor (EDM). GRIMM-
160 SMPS system consists of a Vienna-type monodisperse differential mobility analyzer (M-DMA).
161 DMA classifies the particle according to their electrical mobility, which is then counted using a
162 CPC. EDM uses an Optical Particle Counter (OPC), which works on the light scattering
163 technology for particle counting gives the particle number size distribution in the size range from
164 250 nm to 32 μm (Grimm and Eatough, 2009). Thus, the WRAS system gives the particle number



165 size distribution in the size range from 5.5 nm to 32 μm (72 size bins). The detailed description
166 and principle of the instrument are discussed elsewhere (Grimm and Eatough, 2009). In this study,
167 we used particle number size distributions in the size range of 5.14 nm to 1000 nm from November
168 2011 to January 2013.

169 Mahabaleshwar observation site (MBL, 17.92° N, 73.65° E; 1378 m amsl) is located in the
170 small town named Mahabaleshwar in the forested Western Ghats range in the Satara district of
171 Maharashtra State. In MBL, a High-Altitude Cloud Physics Laboratory (HACPL) was established
172 by the Indian Institute of Tropical Meteorology (IITM), Pune, in 2012, to study monsoon clouds
173 in this region. HACPL site details are found elsewhere (Anil Kumar et al., 2021). Mahabaleshwar
174 town is a tourist attraction consisting of dense vegetation, residential houses, hotels, and a rural
175 market. Pune city is located on the leeward side of the Western Ghats about 100 km to the north,
176 Mumbai city is located approximately 250 km on the northwest, and Satara city is located
177 approximately 50 km to the southeast of Mahabaleshwar. Measurements of particle number size
178 distributions were carried out using the GRIMM-WRAS system. The detailed description and
179 principle of the instrument are discussed elsewhere (Grimm and Eatough, 2009). The sampling
180 probe uses a Nafion dryer to reduce the relative humidity to ~40%. In this study, we used particle
181 number size distributions in the size range of 5.14 nm to 1000 nm from March 2015 to March
182 2016.

183 Hyderabad observation site (HYD, 17.46° N, 78.32° E; 542 m amsl), University of
184 Hyderabad, is located in the outskirts of Hyderabad urban city. HYD observation site details can
185 be found in Sebastian et al. (2021a). Briefly, particle number size distributions in size range from
186 10.9 to 514 nm (108 size bins) were measured using TSI SMPS, which consists of an electrostatic
187 classifier with a long differential mobility analyzer (TSI LDMA, model 3082) and a butanol CPC
188 (TSI, model 3772), on the second floor of the Earth Sciences building located in the University of
189 Hyderabad campus from April 2019 to March 2020. The scanning cycle of SMPS was 300
190 seconds, yielding a particle number size distribution every 5 minutes.

191 Thiruvananthapuram (Trivandrum) observation site (TVM, 8.55° N, 76.97°E, 3 m amsl) is
192 a tropical semi-urban coastal city with a population of ~1 million (Census of India, 2011), located
193 on the southwestern coast of the Indian peninsular. The observations were carried at the Space
194 Physics Laboratory (SPL) within the Thumba Equatorial Rocket Launching Station, which is about
195 500 m due east of the Arabian Sea coast and 10 km northwest of the urban area of



196 Thiruvananthapuram. The experimental site is free from major industrial or urban activities (Babu
197 et al., 2016). TVM station is a part of the Aerosol Radiative Forcing over India (ARFI) project
198 network of the Indian Space Research Organisation - Geosphere-Biosphere Program (ISRO-GBP).
199 Measurements of particle number size distributions in size range from 14.6 nm to 661.2 nm (108
200 size bins) were made using TSI SMPS, which consists of an electrostatic classifier with an LDMA
201 (3081) and a water-based CPC (3786) from January 2013 to January 2014. More details about the
202 site and prevailing meteorology are described in Babu et al. (2016).

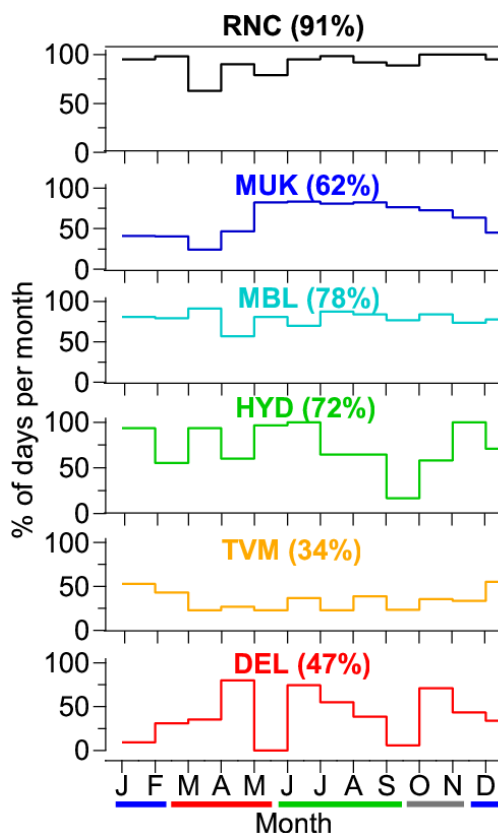
203 Particle number size distributions are categorized by season. We have defined four seasons
204 as indicated in Table 2. The overall particle number size distribution data coverage was adequate
205 (>60 %) at the RNC, MUK, MBL, and HYD sites (Fig. 2) for determining the main seasonal and
206 annual features of particle number size distributions and NPF characteristics. The data coverage at
207 TVM (34%) and DEL (47%) was lower. We also analyzed the number concentration of three sub-
208 micron aerosol modes: Aitken mode (25-100 nm), accumulation mode (100-514 nm), and total
209 particles (<514 nm).

210

211 **Table 2.** Seasons are defined in the analysis and average weather conditions.

Season	Months	Comments
Winter	December, January, February	Cold and dry
Pre-monsoon	March, April, May	Hot and dry
Monsoon	June, July, August, September	Warm, humid, and wet
Post-monsoon	October, November	Cool and humid

212



213

214 **Figure 2.** Particle number size distributions data coverage (% of days/month) at the sites. The
215 values in the bracket indicate total data coverage. The blue, red, green, and grey colored thick lines
216 indicate winter, pre-monsoon, monsoon, and post-monsoon months.

217

218 2.2 New particle formation event classification and features

219 We classified observation days into three types of events: NPF event day, non-event day,
220 and undefined event day using visual inspection of the particle number size distributions following
221 the methodology given by Dal Maso et al. (2005). A day was classified as an NPF event day by
222 the presence of a distinctly new mode of particles with a diameter smaller than 25 nm and steady
223 growth in diameter of this new mode such that the particle number size distributions display a
224 noontime "banana" shaped aerosol growth. The particle mode diameter (i.e., the local maximum
225 of the particle number size distribution) was obtained by fitting a log-normal distribution to the
226 measured particle number size distribution. A day without any evidence of a distinctly new mode



227 of particles diameter smaller than 25 nm was identified as a non-event day. Those days, which
228 were difficult to be classified as any one of the above two event types, were identified as undefined
229 event days. For NPF events, the particle growth rate (GR) was calculated by fitting a first-order
230 polynomial line through growing particle mode diameter between the lowest detectable size (LDS)
231 of the instrument (e.g., 10 nm for RNC) and 25 nm as a function of time and calculating its slope.
232 The formation rate of a particle at the LDS (J_{LDS}) was also found using the simplified
233 approximation of the General Dynamic Equation (GDE), describing the evolution of the particle
234 number size distribution as given below;

235

$$236 \quad J_{LDS} = \frac{dN_{LDS-25}}{dt} + F_{CoagS} + F_{growth} \quad (1)$$

237

238 where the first term in Eq. (1) is the rate of the change of nucleation mode particle number
239 concentrations, the second term is the coagulation loss of nucleation mode particles, and the third
240 term is the flux out of the size range of LDS-25 nm, i.e., condensational growth (Dal Maso et al.,
241 2005). A direct comparison of GR and J between all of the sites is not possible because of the
242 different size ranges covered by the instruments.

243

244 **2.3 Increase in CCN concentrations from NPF**

245 The increase in CCN concentrations from any given NPF event can be estimated by
246 comparing the CCN concentration before the event ($N_{CCNprior}$) and the maximum CCN
247 concentration during the event (N_{CCNmax}) following the methodology developed by Kerminen et
248 al. (2012), which we modified further. In typical ambient in-cloud supersaturations, the total
249 number of particles from 50 nm to >100 nm can be considered as a proxy for CCN concentrations
250 (Westervelt et al., 2013; Kerminen et al., 2012). $N_{CCNprior}$ was chosen to be a one-hour average
251 concentration of particles larger than 50 nm (and 100 nm) just before the start of the NPF event.
252 N_{CCNmax} was taken as a maximum one-hour average concentration of particles larger than 50 nm
253 (and 100 nm) during the event. The N_{CCNmax} is not the best representation of CCN concentration
254 after the NPF event because it is not possible to estimate the end of an NPF event. But it gives a
255 rough estimate of the observed maximum number of primary and secondary particles present in
256 the atmosphere during an event (Kerminen et al., 2012). We calculated the seasonally averaged
257 change in CCN-active particles on non-event days over the same time of day as the NPF events,



258 which would account for the CCN concentrations from processes other than NPF. Then, the
259 absolute increase in CCN concentration from NPF is calculated as given below,

260

$$261 \text{ CCN increase} = (N_{\text{CCNmax}} - N_{\text{CCNprior}})_{\text{NPFevent}} - (N_{\text{CCNmax}} - N_{\text{CCNprior}})_{\text{non-events}} \quad (2)$$

262

263 The first term on the right-hand side in Eq. (2) indicates the CCN increase during an NPF event,
264 while the second term indicates the CCN increase during a non-event. This difference between
265 them allows us distinguishing primary particles and particles formed originally from atmospheric
266 nucleation and yields the best representation of CCN concentrations after the NPF event. But the
267 atmospheric condition on non-event days is generally different from NPF event days; therefore,
268 the calculated increase in CCN concentrations from NPF may be imprecise.

269

270 **3. Results and discussion**

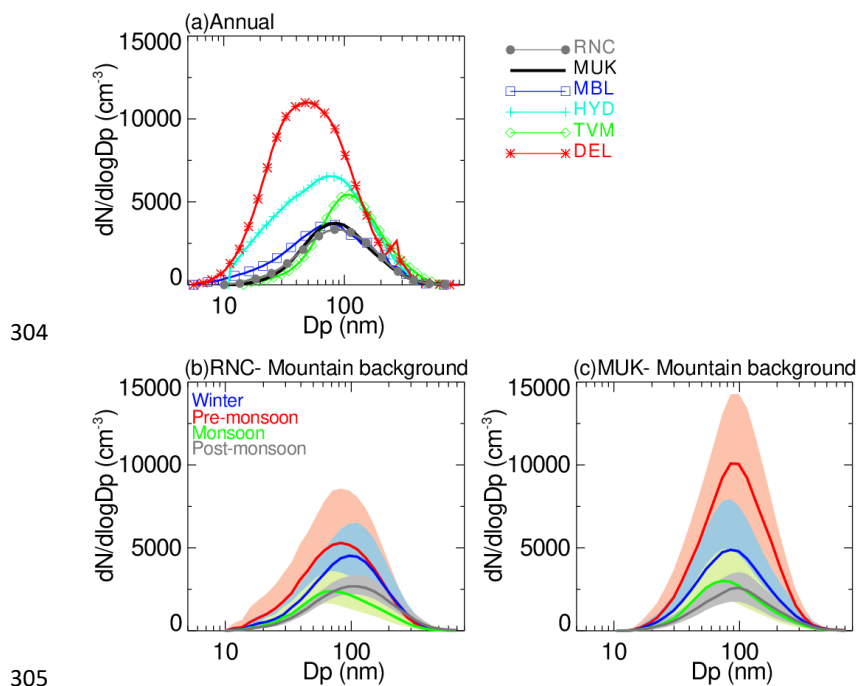
271 **3.1 Variability in particle number size distributions and number concentrations**

272 Figure 3 shows the annual and seasonal median and 25th and 75th percentile values of
273 particle number size distributions at all the sites. The thick line represents the median value,
274 whereas the shaded area indicates particle number size distribution between 25th and 75th
275 percentiles. The annual median particle number size distribution has the smallest mode diameter
276 at DEL compared to the other sites. The smallest mode diameter necessarily indicates the
277 significant near-surface anthropogenic sources at DEL as compared to other sites. The mountain
278 sites (RNC, MUK, and MBL) all show similar mode diameters, with the lowest concentrations at
279 RNC. Amongst urban areas (HYD, TVM, and DEL), TVM has the largest mode diameter, which
280 is frequently influenced by the influx of marine air masses containing high moisture and coarser
281 sea salt aerosols (Babu et al., 2016) (Fig. 3a). The peak number concentration of PNSDs is the
282 highest in pre-monsoon (MAM) than in other seasons at RNC and MUK (Fig. 3b-c), while it was
283 similar in winter and pre-monsoon at MBL (Fig. 3d). These elevated concentrations are
284 accompanied by a smaller mode diameter of the Aitken mode particles. The highest number
285 concentration is attributed to the frequent occurrence of NPF in these locations in pre-monsoon
286 (Sebastian et al., 2021b; Neitola et al., 2011). The contribution of newly formed particles to total
287 particles is also visible in the 75th percentile PNSDs at these sites. The number size distributions
288 of particles were significantly the lowest in monsoon and post-monsoon.



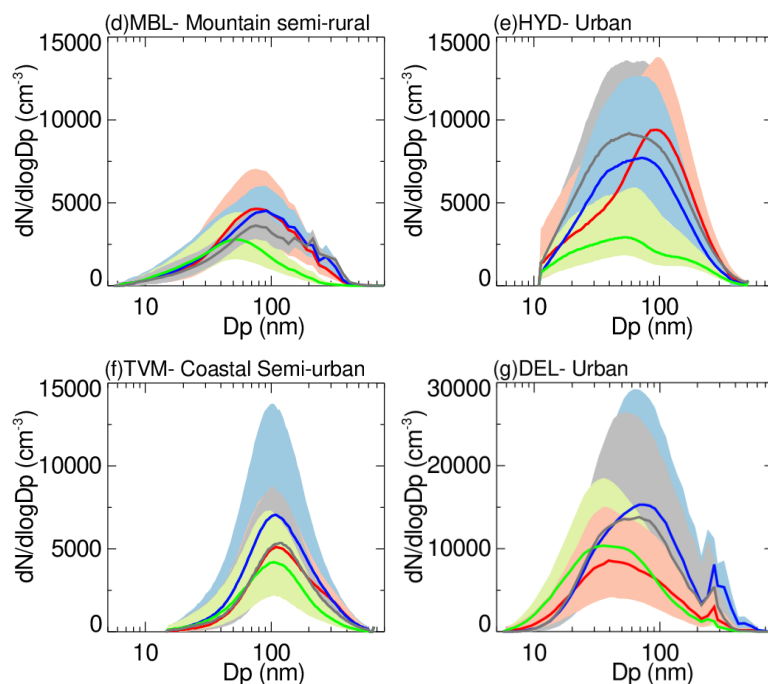
289 The median number size distribution of particles at HYD is the highest in pre-monsoon
290 and post-monsoon (Fig. 3e). The highest particle number concentrations in pre-monsoon and post-
291 monsoon can be attributed to the frequent occurrence of NPF in these seasons at the site. The
292 influence of NPF is also noticeable in the 75th percentile PNSDs. The PNSD is consistently the
293 lowest in monsoon, attributed to the wet scavenging of particles. The concentrations of Aitken and
294 accumulation mode particles are the highest in winter compared to the other seasons. The mode
295 diameter of PNSDs at TVM is comparatively similar in all seasons (Fig. 3f). At DEL, the mode
296 diameter of PNSDs is the highest in winter compared to the other seasons (Fig. 3g). The shallow
297 boundary layer height, stagnant atmospheric conditions, and high emission rates of aerosol
298 precursors in winter (Kanawade et al., 2020b) allow particles to stay close to the surface and grow
299 larger under high relative humidity and high condensable vapor concentrations. The median PNSD
300 is consistently the lowest in monsoon at TVM due to extensive wet scavenging. The strong
301 seasonality in PNSDs is similar to those reported earlier in India (Hooda et al., 2018; Kompulla
302 et al., 2009; Gani et al., 2020; Kanawade et al., 2014a).

303





306



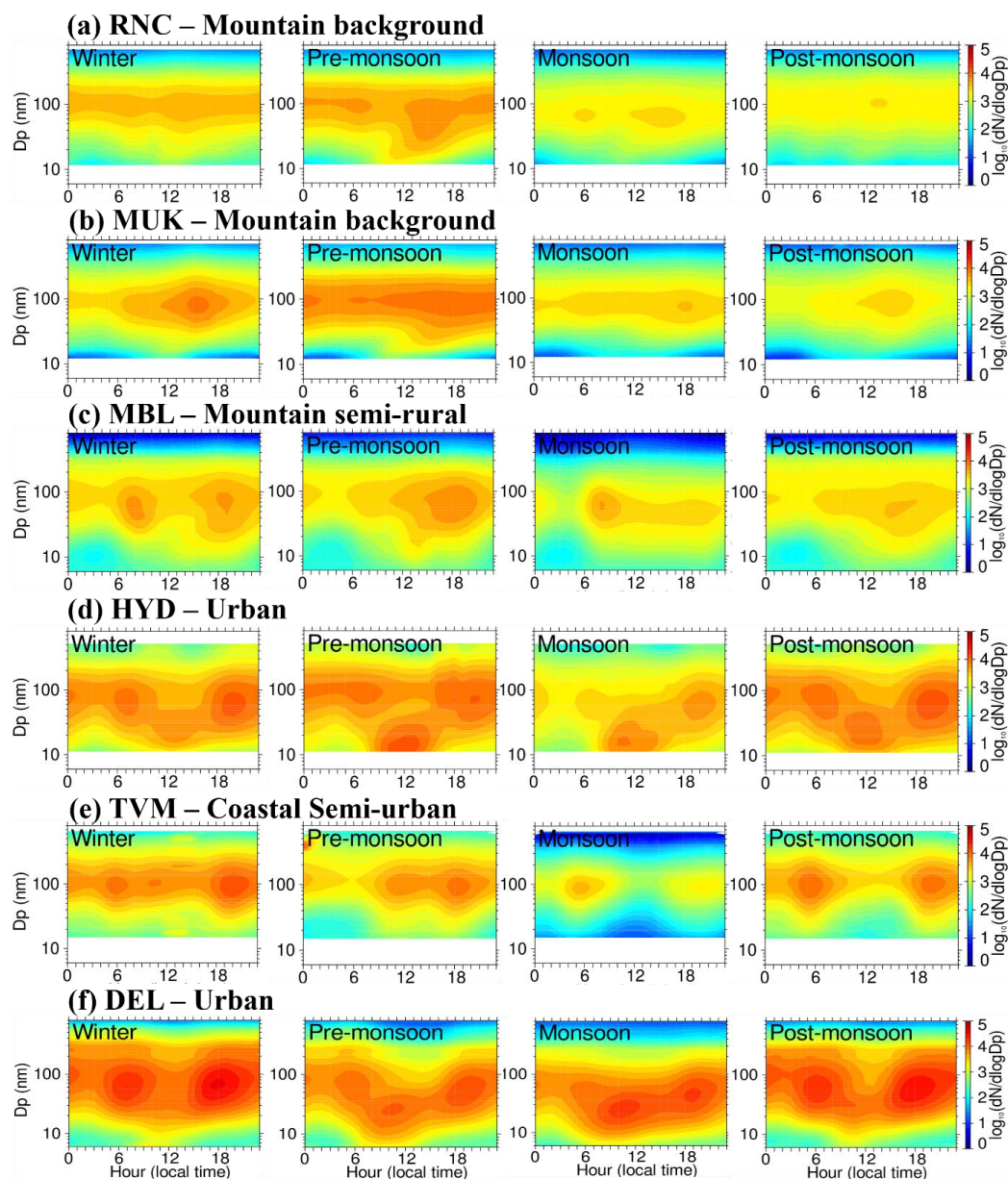
307

308 **Figure 3.** (a) Annual and (b-g) seasonal median particle number size distributions at all the sites.
309 The solid line indicates the median, and the light-colored shading indicates 25th and 75th percentile
310 distributions. The blue line and shading indicate winter (DJF), red line and shading indicate pre-
311 monsoon (MAM), green line and shading indicate monsoon (JJAS), and grey line and shading
312 indicate post-monsoon season (ON). Note that the y-axis scale is different for the DEL site.

313

314 Figure 4 shows the average observed PNSDs evolving over the day for each season, as a
315 contour plot, at all the sites. For RNC and MUK, the average seasonal contour plot indicates
316 daytime NPF in pre-monsoon. However, winter, monsoon, and post-monsoon had the lowest
317 concentrations of smaller particles that are not associated with NPF. For MBL, NPF occurred in
318 winter, pre-monsoon, and post-monsoon. For all urban sites (HYD, TVM, and DEL), the average
319 seasonal contour plot indicates the highest concentration of particles in morning and evening peak
320 traffic hours, in addition to daytime NPF. In Section 3.2, we investigate the frequency of
321 occurrence of NPF and its contribution to CCN concentrations.

322



323

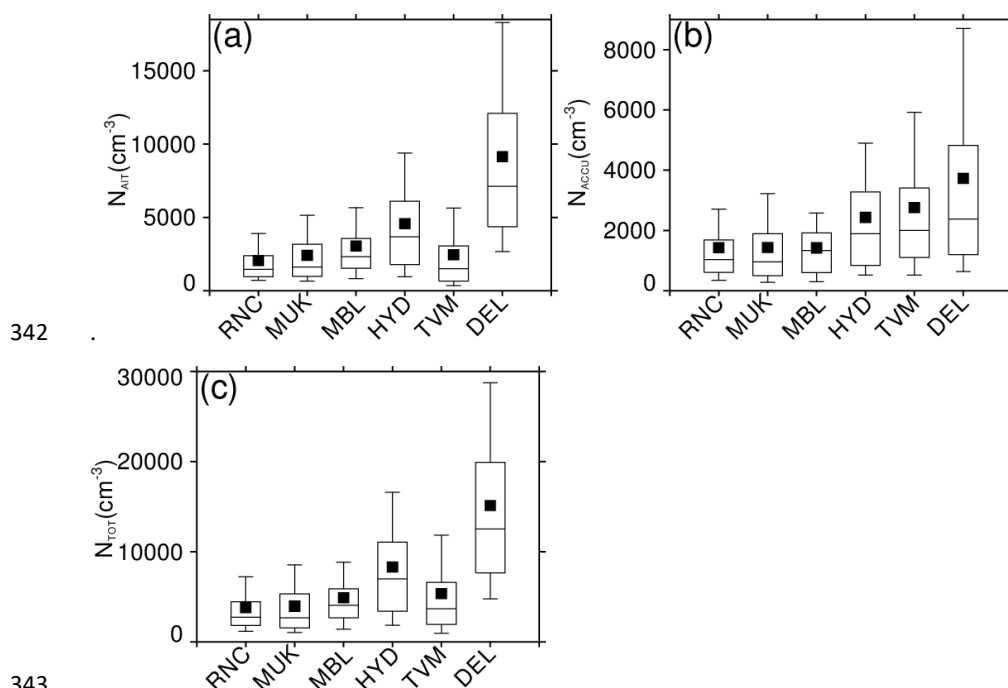
324 **Figure 4.** The diurnal-seasonal median particle number size distributions at all the sites; a)
325 Ranichauri, b) Mukteshwar, c) Mahabaleshwar, d) Hyderabad, e) Thiruvananthapuram, and f)
326 Delhi.

327



328 Figure 5 shows the box-whisker plot of the number concentrations of Aitken,
329 accumulation, and total particles at all the sites. The median Aitken mode particle number
330 concentrations are the lowest at RNC ($1.4 \times 10^3 \text{ cm}^{-3}$) and the highest at DEL ($7.1 \times 10^3 \text{ cm}^{-3}$). The
331 median accumulation mode particle number concentrations are the lowest at MUK ($0.9 \times 10^3 \text{ cm}^{-3}$)
332 and the highest at DEL ($2.4 \times 10^3 \text{ cm}^{-3}$). The total particle number concentrations are the lowest at
333 MUK ($2.7 \times 10^3 \text{ cm}^{-3}$) and the highest at DEL ($12.5 \times 10^3 \text{ cm}^{-3}$). The median particle number
334 concentrations are about 5-fold higher in urban locations (HYD, TVM, and DEL) than mountain
335 sites (RNC, MUK, and MBL). Overall, the size-segregated particle number concentrations show
336 strong spatial variability, with the lowest concentrations at the mountain sites and the highest at
337 the urban sites. Further, the size-segregated particle number concentrations also show the large
338 variability in each urban location than the mountain sites. Next, we discuss the seasonality in the
339 number concentration of Aitken, accumulation, and total particles in all locations to understand
340 space- and time-varying heterogeneity in particle number concentrations.

341



344 **Figure 5.** Box-whisker plot of the size-segregated particle number concentrations using the entire
345 data. The filled square indicates the mean, the horizontal line indicates the median, the top and



346 bottom of the box indicate 25th and 75th percentile values, and the top and bottom whiskers indicate
347 10th and 90th percentile values.

348

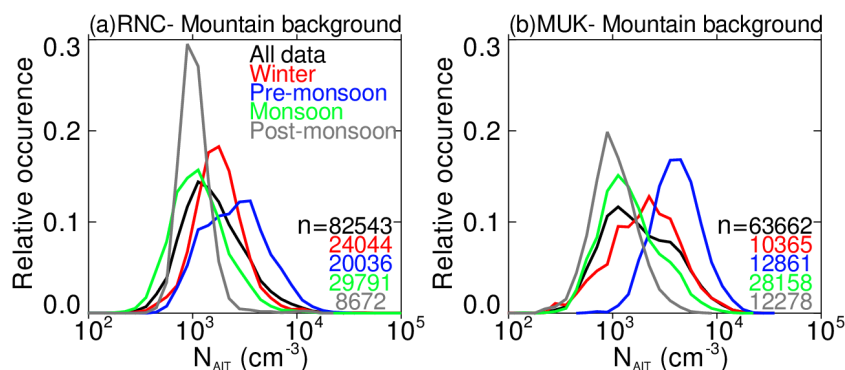
349 The histograms of the relative occurrence of Aitken mode particle number concentrations
350 at all the sites are presented in Figure 6(a-f). RNC and MUK show a similar seasonality in number
351 concentration histograms of Aitken mode particles, with a reasonably log-normal shape and the
352 highest concentrations in the pre-monsoon season. The lowest concentrations are observed in
353 monsoon and post-monsoon due to increased removal of particles by wet-scavenging. MBL does
354 not show notable seasonality in the number concentration histograms of Aitken mode particles.
355 HYD, TVM, and DEL are urban environments but show different seasonality in the number
356 concentration histograms of Aitken mode particles. DEL shows the highest Aitken mode particle
357 number concentrations in winter, and post-monsoon, TVM show the highest concentrations in
358 winter. In contrast, HYD shows comparable number concentrations in winter, pre-monsoon, and
359 post-monsoon. The highest Aitken mode number concentrations in pre-monsoon at mountain-
360 background sites are attributed to the high frequency of NPF occurrence in pre-monsoon (see Sect.
361 3.2.1). The highest Aitken mode number concentrations in winter at urban sites can be explained
362 by the high pre-existing particle concentration. The difference in seasonality in the number
363 concentration histograms of Aitken mode particles can be explained by the differences in the
364 atmospheric conditions (e.g., prevailing synoptic air masses, mesoscale processes such as
365 atmospheric boundary layer dynamics, and particle removal processes) and considerable
366 heterogeneity in aerosol composition (natural versus anthropogenic aerosol emission sources);
367 DEL is representative of a sub-tropical climate, HYD is representative of a tropical climate, and
368 TVM is representative of a tropical-coastal climate.

369

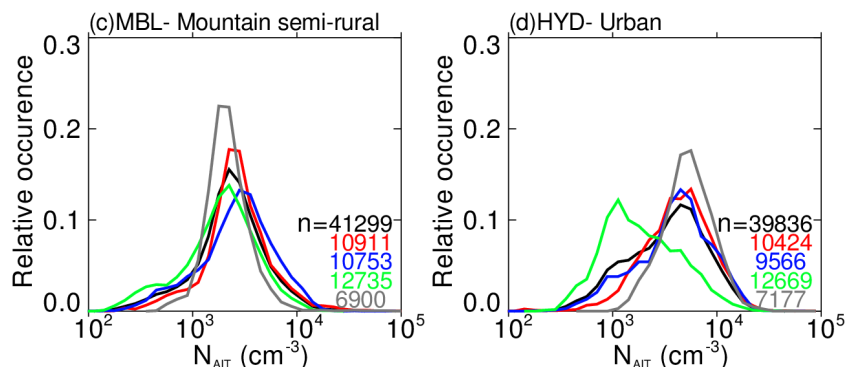
370



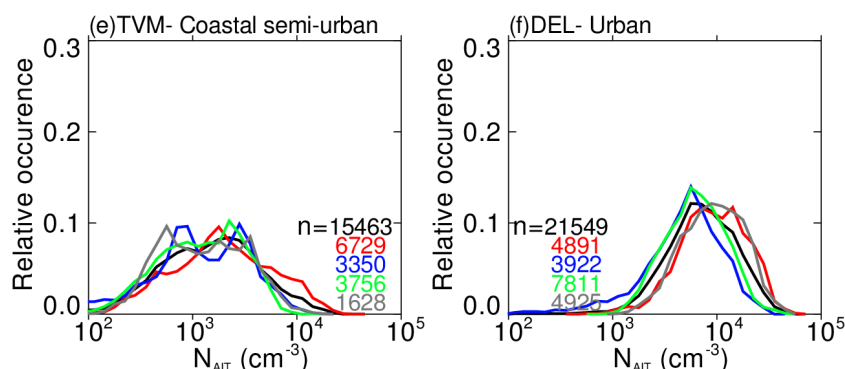
371



372



373



374 **Figure 6.** Histogram of the relative occurrence of Aitken mode particle number concentrations at
 375 the sites. The concentration bins are logarithmically spaced in the x-axis, and the y-axis shows the
 376 relative occurrence of values in each bin compared to the total number of valid observations. The
 377 thick black line indicates all data. The red, blue, green, and grey lines indicate winter (DJF), pre-
 378 monsoon (MAM), monsoon (JJAS), and post-monsoon (ON) months. n indicates the number of
 379 10 minutes averaged valid data points.

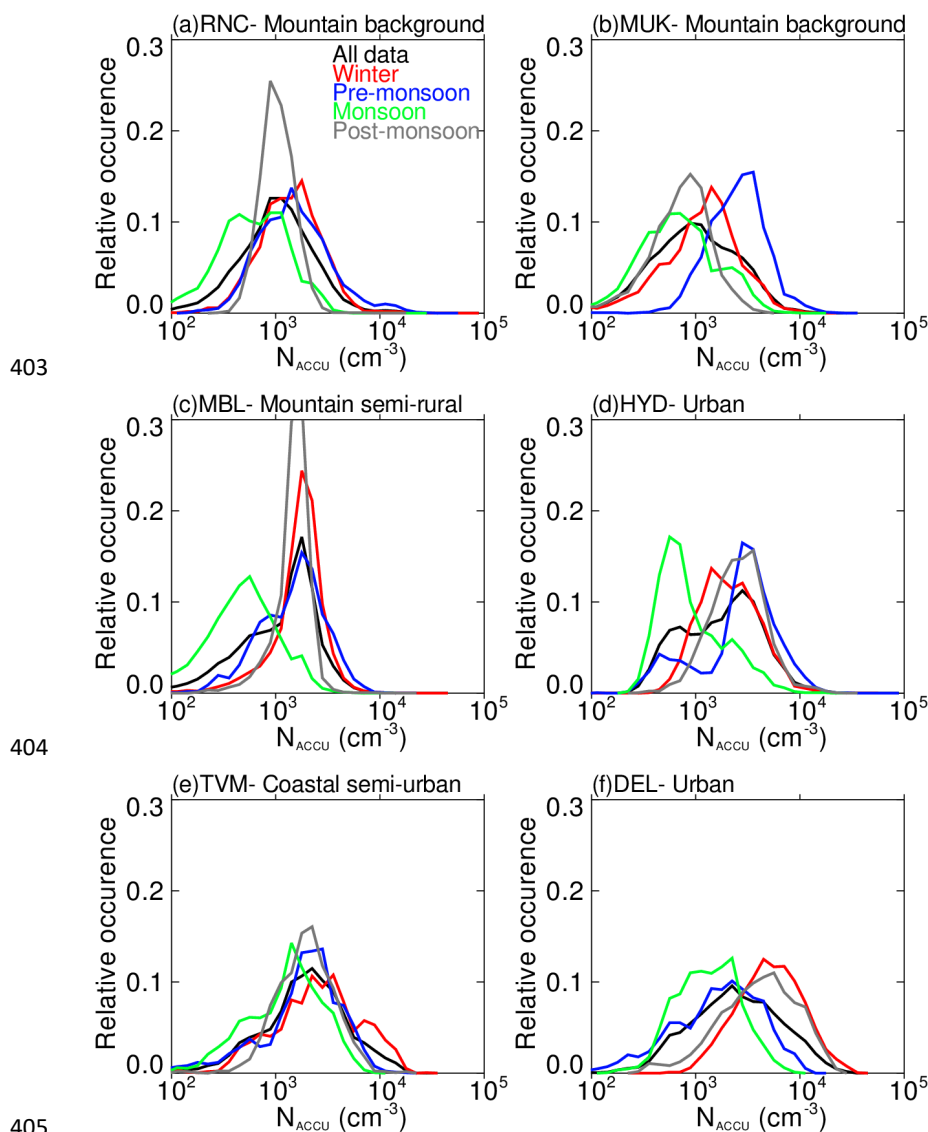
380



381 Similar histograms of accumulation mode particles are presented in Fig. 7(a-f). The
382 seasonality in accumulation mode particles is slightly different as compared to Aitken mode
383 particles at some sites. RNC shows similar number concentration histograms of accumulation
384 mode particles in winter and pre-monsoon instead of dissimilar histograms for Aitken mode
385 particles. The number concentration histograms of accumulation mode particles at MUK are
386 similar to Aitken mode particles. MBL shows similar number concentration histograms in winter,
387 pre-monsoon, and post-monsoon, with the lowest concentrations in monsoon due to wet
388 scavenging. Among the urban sites, DEL shows the highest accumulation mode concentrations in
389 post-monsoon and winter. TVM and HYD show the highest accumulation mode concentrations in
390 winter and post-monsoon, respectively. The seasonality in total particles was also similar to Aitken
391 mode particles, indicating that Aitken mode particles constituted the most considerable fraction of
392 total particles at all the sites (Figure not shown). However, it is difficult to separate a fraction of
393 Aitken or accumulation mode particles that originated from NPF from that of the primary
394 emissions, especially in urban areas where the primary emission rates of aerosols are very high
395 (Thomas et al., 2019). The survival probability of newly formed particles to >50-100 nm size
396 depends on many factors such as the frequency and intensity of the NPF occurrence, availability
397 of condensable vapors, pre-existing particles, and atmospheric conditions. In Sect. 3.2.3, we
398 estimate the absolute increase of CCN concentrations from NPF following the methodology given
399 by Kerminen et al. (2012) and modified to remove the possible contribution from the primary
400 particles to CCN concentrations for any given NPF event.

401

402



406 **Figure 7.** Same as Fig. 6, but for accumulation mode particle number concentrations.

407

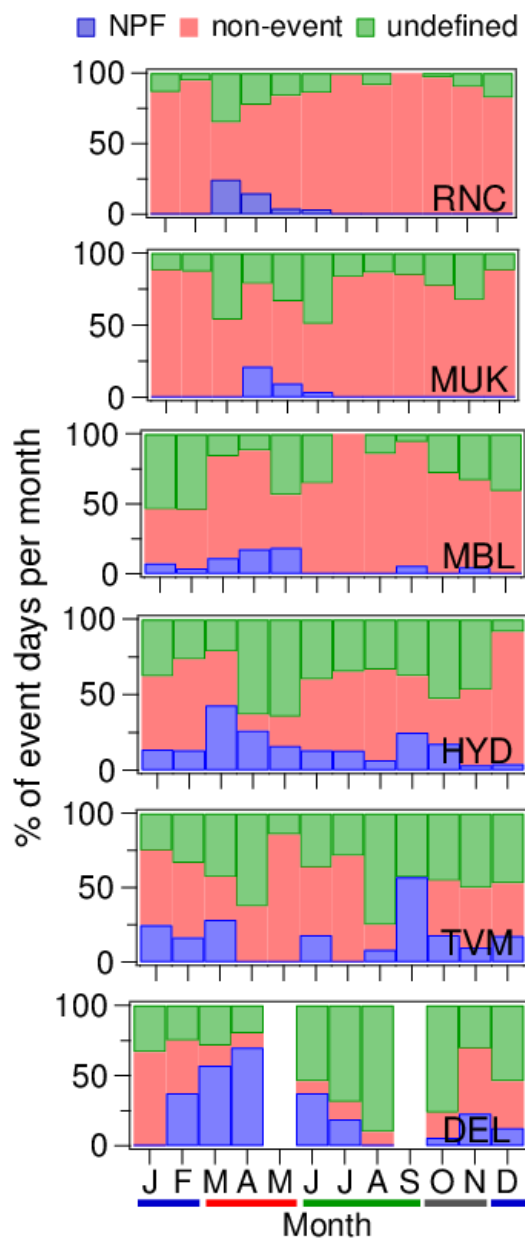
408 3.2 New particle formation and its contribution to CCN concentrations

409 3.2.1 NPF event characteristics

410 The frequency of occurrence of NPF events, the particle formation rate of nucleation mode
411 particles (J_{NUC}), and the particle growth rate of nucleation mode particles (GR_{NUC}) are typically
412 derived to quantify the NPF (Kerminen et al., 2018; Nieminen et al., 2018; Kulmala et al., 2004).



413 These NPF characteristics are closely associated with aerosol precursor concentrations, pre-
414 existing aerosol particles, and atmospheric conditions. As a result, the frequency of occurrence of
415 NPF events varies from one location to another as well as seasonally. NPF is thought to occur
416 frequently during the spring (pre-monsoon) and rarely during the winter (Kanawade et al., 2012;
417 Dal Maso et al., 2005; Nieminen et al., 2018). However, NPF events were also observed frequently
418 during the thermal winter (Kulmala et al., 2004; Pikridas et al., 2012) and fall (September, October,
419 and November) (Rodríguez et al., 2005). These studies indicate that there is no universal pattern
420 in the occurrence of NPF events. Figure 8 shows the percentage of NPF, non-event, and undefined
421 event days based on valid observation days at all the sites. Out of a total of 586 valid observation
422 days at RNC, NPF events occurred on 21 days (3.9%), whereas 493 (83.7%) days were non-event
423 days. Out of a total of 440 valid observation days at MUK, NPF events occurred on 13 days (2.9%),
424 whereas 321 (73.1%) days were non-event days. Out of a total of 281 valid observation days at
425 MBL, NPF events occurred on 16 days (5.9%), whereas 188 (66.1%) days were non-event days.
426 Out of a total of 270 valid observation days at HYD, NPF events occurred on 38 days (16.3%),
427 whereas 124 (44.8%) days were non-event days. Out of a total of 133 valid observation days at
428 TVM, NPF events occurred on 23 days (16.6%), whereas 55 (41.4%) days were non-event days.
429 Out of a total of 139 valid observation days at DEL, NPF events occurred on 39 days (28.1%),
430 whereas 30 (21.1%) days were non-event days.



431

432 **Figure 8.** Monthly percentage of occurrence of NPF, non-event, and undefined events days based
433 on total valid observations days at all the sites. The blue, red, green, and grey colored thick lines
434 indicate winter, pre-monsoon, monsoon, and post-monsoon months.

435



436 **3.2.2 Particle formation rate and growth rate**

437 Overall, the frequency of occurrence of NPF is the highest in pre-monsoon as compared to
438 other seasons. There is also an exception to this, with the highest frequency of NPF occurrence in
439 the late monsoon (September) at TVM. Babu et al. (2016) have reported that NPF events over this
440 site occurred due to a mixing of contrasting air masses due to the combined effect of mesoscale
441 land-sea breeze circulation and local ABL dynamics. Though prevailing air masses are oceanic,
442 the wind speeds and total rainfall were lower during September than other monsoonal months. A
443 cleaner synoptic air mass (i.e., lower background concentrations and condensation sink), combined
444 with the occurrence of well-defined mesoscale land-sea breeze transitions and horizontal
445 convergence of contrasting air masses during September, was responsible for the highest NPF
446 frequency. Amongst the sites, the mountain-background sites in the Western Himalaya (RNC and
447 MUK) have the lowest annual mean frequency of occurrence of NPF (3.9% and 2.9%,
448 respectively), with the highest seasonal frequency of occurrence of NPF in pre-monsoon. Previous
449 studies also showed the infrequent occurrence of NPF at RNC (Sebastian et al., 2021b) and MUK
450 (Neitola et al., 2011), with the highest frequency in pre-monsoon. The highest NPF frequency in
451 pre-monsoon was connected to the planetary boundary layer uplifting to the measurement site
452 elevation that appeared to transported aerosol precursors from nearby polluted lower-altitude
453 regions (Hooda et al., 2018; Raatikainen et al., 2014). However, NPF occurred frequently (39%)
454 at the Nepal Climate Observatory-Pyramid (NCO-P) site in the Eastern Himalaya (Venzac et al.,
455 2008). A recent study also observed a very high NPF frequency (69%) at NCO-P from November
456 to December when cleaner conditions prevailed, with little transportation from the polluted lower-
457 altitude regions (Bianchi et al., 2021). They showed that up-valley winds bring gaseous aerosol
458 precursors to higher altitudes. These precursors are oxidized into compounds of very low volatility
459 and are subsequently converted into new particles during their transport to the site. The above
460 discussion indicates that RNC and MUK mountain-background sites in the Western Himalayas are
461 strikingly different from the NCO-P site in the Eastern Himalayas (Bianchi et al., 2021). The
462 annual NPF frequency at RNC and MUK is lower than MBL and the high-altitude sites in Europe
463 (Nieminen et al., 2018). DEL has the highest frequency of occurrence of NPF events in pre-
464 monsoon (63.8%), followed by HYD (28.4%) and MBL (15.9%). TVM coastal semi-urban site
465 witnesses frequent NPF events under the influence of continental air masses. As the air masses
466 change from continental to mixed or marine origin, the NPF event frequency decreases (Babu et

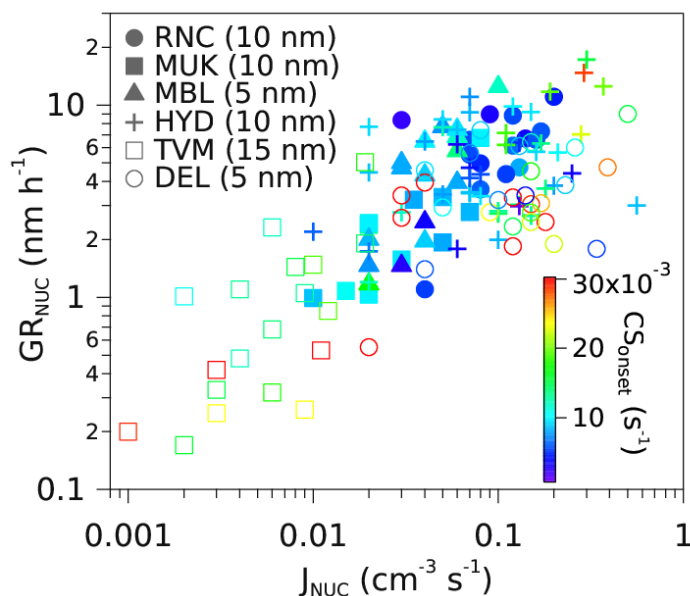


467 al., 2016). NPF was also observed commonly at other urban sites in India (Kanpur and Pune) under
468 a high source of aerosol precursors when pre-existing particle concentrations reduced sufficiently
469 due to dilution (Kanawade et al., 2020a; Kanawade et al., 2014b). While the severe air pollution
470 episode in Delhi in November 2016 suppressed the NPF, the co-condensation of vapors of
471 anthropogenic origin along with water onto primary particles assisted the rapid particle growth
472 (1.6 to 30.3 nm h⁻¹) (Kanawade et al., 2020b). The emission of precursor compounds from traffic
473 and other sources in Beijing, China, also contributed significantly to the molecular cluster
474 formation, particle growth and secondary aerosol mass formation, leading to haze formation under
475 favorable meteorological conditions (Kulmala et al., 2021). In Europe, the atmospheric conditions
476 (such as the solar radiation and relative humidity) appear to dictate the NPF occurrence at rural
477 sites, whereas the increased concentrations of precursor gases are more important for the
478 occurrence of NPF in urban areas (Bousiotis et al., 2021). This explains why NPF occurs more
479 frequently in urban areas than rural, remote or high-altitude locations (Guo et al., 2020; Nieminen
480 et al., 2018; Sellegri et al., 2019). This also indicates that the balance between the precursor
481 concentration and pre-existing particles plays a vital role in the NPF occurrence. Owing to large
482 spatial heterogeneity in aerosol precursor emissions and background aerosol concentrations in
483 India, the chemical species contributing to aerosol nucleation and growth is unidentified
484 (Kanawade et al., 2021). The atmospheric NPF can be quantified by calculating J_{NUC} and GR_{NUC}
485 for the observed NPF events, which we discuss next.

486 Figure 9 shows the scatter plot of the J_{NUC} and the GR_{NUC} as a function of condensation
487 sink at each site. A fairly good correlation between J_{NUC} and GR_{NUC} at each site (Pearson
488 correlation coefficient of 0.48, 0.78, 0.85, 0.33, 0.68, and 0.18 at RNC, MUK, MBL, HYD, TVM,
489 and DEL, respectively) indicates that J_{NUC} and GR_{NUC} are strongly coupled. The large scatter in
490 data points is a result of important factors influencing the NPF, such as nucleation mechanisms
491 (Dunne et al., 2016), the availability of other condensable vapors that are needed to stabilize
492 molecular clusters containing sulfuric acid (Kirkby et al., 2011; Schobesberger et al., 2015), and
493 atmospheric conditions (Bousiotis et al., 2021). A recent study showed that amines stabilize the
494 nucleating cluster while organics contribute to higher concentrations of condensable vapors,
495 particularly in urban areas (Xiao et al., 2021). The formation rate of 10 nm particles at mountain-
496 background sites (RNC and MUK) varied from 0.01 to 0.1 cm⁻³ s⁻¹, with a mean value of 0.08 cm⁻³
497 s⁻¹. The formation rate of 5 nm particles at MBL varied from 0.02 to 0.1 cm⁻³ s⁻¹, with a mean of



498 $0.04 \text{ cm}^{-3} \text{ s}^{-1}$. The formation rate of 10 nm particles at HYD varied from 0.01 to $0.56 \text{ cm}^{-3} \text{ s}^{-1}$, with
499 a mean of $0.13 \text{ cm}^{-3} \text{ s}^{-1}$. The formation rate of 15 nm particles at TVM varied from 0.001 to 0.02
500 $\text{cm}^{-3} \text{ s}^{-1}$, with a mean of $0.07 \text{ cm}^{-3} \text{ s}^{-1}$. The formation rate of 5 nm particles at DEL varied from
501 0.01 to $0.5 \text{ cm}^{-3} \text{ s}^{-1}$, with a mean value of $0.12 \text{ cm}^{-3} \text{ s}^{-1}$. The mean growth rates of nucleation mode
502 particles during NPF events were 6.3 nm h^{-1} , 2.5 nm h^{-1} , 4.7 nm h^{-1} , 5.7 nm h^{-1} , 1.1 nm h^{-1} , and 3.7
503 nm h^{-1} , at RNC, MUK, MBL, HYD, TVM, and DEL, respectively. Considering all the sites, GR_{NUC}
504 during NPF events varied from 0.2 to 17.2 nm h^{-1} . Overall, J_{NUC} and GR_{NUC} are within the observed
505 large range of values in diverse environments in India and elsewhere (Nieminen et al., 2018;
506 Kerminen et al., 2018; Kulmala et al., 2004). Expectedly, the condensation sink at the start of the
507 NPF event is higher at urban sites than the mountain sites. The mean condensation sink at urban
508 sites ($16.1 \times 10^{-3} \text{ s}^{-1}$) was twice as compared to mountain sites ($7.9 \times 10^{-3} \text{ s}^{-1}$). A previous study also
509 showed that the higher pre-existing particles at Kanpur than at Pune suppressed the particle
510 formation rate but favored the particle growth under high concentrations of condensable vapors
511 (Kanawade et al., 2014b)



512
513 **Figure 9.** Scatter plot of the particle formation rate and the growth rate as a function of
514 condensation sink at each site. The condensation sink is taken at the start of the NPF event. The
515 lowest nucleation mode detectable size at each site is shown in the bracket.
516



517 3.2.3 Increase in CCN concentrations during NPF events

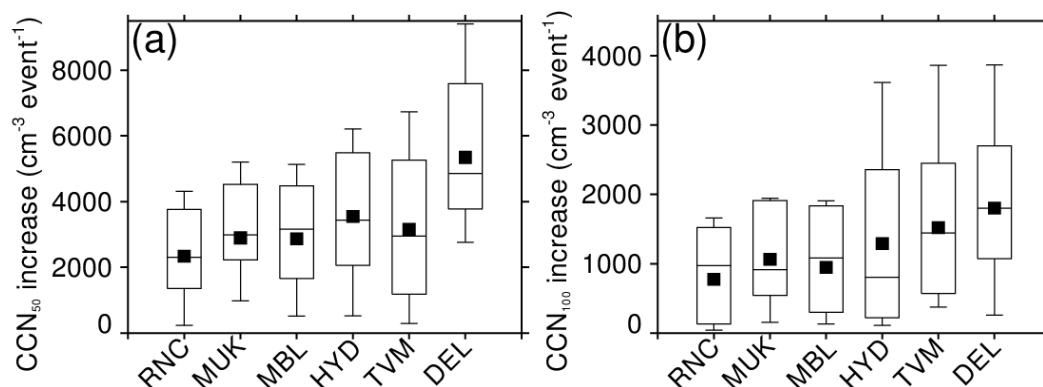
518 To reach climatologically relevant sizes, the newly formed particles must grow by
519 condensation while avoiding coagulation removal by pre-existing particles because these freshly
520 formed particles are small and highly diffusive (Vehkamäki and Riipinen, 2012). Based on the
521 observed range of particle growth rates at all the sites (0.2 to 17.3 nm h⁻¹), newly formed particles
522 may take from a few hours to 1-2 days to grow to CCN-active sizes (>50-100 nm). Over such time
523 scales, it is observationally challenging to separate CCN originating from NPF from those
524 emanating from the growth of small primary particles and direct emission of CCN-active sized
525 particles. The increase in CCN concentrations during any given NPF event was estimated
526 following the methodology developed by Kerminen et al. (2012), which we modified to remove
527 CCN originating from the growth of small primary particles and direct emission of CCN-active
528 sized particles based on non-event days.

529 Figure 10 shows the box-whisker plot of the absolute increase in CCN concentrations (50
530 and 100 nm) at all the sites. Considering all NPF events at mountain sites, increase in CCN₅₀
531 ranged from 168 cm⁻³ per event to 5.2×10^3 cm⁻³ per event, with a median value of 2.7×10^3 cm⁻³
532 per event, whereas the increase in CCN₁₀₀ ranged from 0.02×10^3 cm⁻³ per event to 1.9×10^3 cm⁻³
533 per event, with the median value of 1.0×10^3 cm⁻³ per event. The increase in CCN₅₀ and CCN₁₀₀ is
534 about two-fold lower than the free tropospheric site, Chacaltaya (5240 m amsl, Bolivia), for NPF
535 events started in the boundary layer (5.1×10^3 cm⁻³ per event and 1.5×10^3 cm⁻³ per event for 50 and
536 100 nm, respectively) (Rose et al., 2017). The median increase in CCN₅₀ and CCN₁₀₀ at RNC
537 (2.3×10^3 cm⁻³ per event and 0.9×10^3 cm⁻³ per event) and MUK (2.9×10^3 cm⁻³ per event and 0.9×10^3
538 cm⁻³ per event) are comparable to those reported at Botsalano (1420 m amsl, South Africa);
539 2.5×10^3 cm⁻³ per event and 0.8×10^3 cm⁻³ per event, respectively, but about three-fold higher than
540 those reported at a remote continental site in Finland (1.0×10^3 cm⁻³ per event and 0.2×10^3 cm⁻³ per
541 event for 50 nm and 100 nm, respectively) (Kerminen et al., 2012). Considering all NPF events at
542 the urban sites, CCN₅₀ increase ranged from 0.08×10^3 cm⁻³ per event to 9.4×10^3 cm⁻³ per event,
543 with a median value of 4.3×10^3 cm⁻³ per event, whereas CCN₁₀₀ increase ranged from 0.03×10^3
544 cm⁻³ per event to 4.9×10^3 cm⁻³ per event, with a median value of 1.2×10^3 cm⁻³ per event. These
545 values are about two-folds lower as compared to values reported at the station of San Pietro
546 Capofiume, in a polluted region of the Po Valley; 7.3×10^3 cm⁻³ per event and 2.4×10^3 cm⁻³ per
547 event, respectively for 50 nm and 100 nm (Laaksonen et al., 2005). The overall effect of NPF



548 events on the CCN concentrations at DEL was the largest since the high background number
549 concentrations of CCN_{50} and CCN_{100} resulted in a smaller relative increase, particularly in post-
550 monsoon and winter seasons when compared to the other sites. In order to comprehensively
551 investigate the atmospheric CCN budget and the contribution of NPF to it, Kerminen et al. (2012)
552 pointed out that the analysis should include not only NPF events but also non-event days.
553 Therefore, the modified methodology applied here following Kerminen et al. (2012) provides the
554 best representative of the increase in CCN concentrations for an NPF event.

555



556

557

558 **Figure 10.** Box-whisker plot of absolute increase in CCN concentrations for (a) 50 nm and (b) 100
559 nm particles at all the sites based on the observed NPF and non-event events. The filled square
560 indicates the mean, the horizontal line indicates the median, the top and bottom of the box indicate
561 25th and 75th percentile values, and the top and bottom whiskers indicate 10th and 90th percentile
562 values.

563

564 The sites with low pre-existing particle concentrations (hence, low condensation sink
565 values), high solar radiation, and cooler temperatures at high-altitude (or free tropospheric) (RNC,
566 MUK, and MBL) should favor NPF with enhanced frequency as compared to near-surface urban
567 environments (HYD, TVM, and DEL) wherein pre-existing particles concentration are high,
568 leading to faster removal of nucleating vapors. However, NPF in polluted environments occurs
569 more often than expected, with enhanced growth rates (Yu et al., 2017). Guo et al. (2014) also
570 reported that NPF leads to winter-time haze formation in Beijing. Kulmala et al. (2021) recently
571 showed that >65% of the number concentration of haze particles resulted from NPF in Beijing.



572 The observation sites at altitudes higher than 1000 m amsl also favored NPF at the high
573 condensation sinks and linked precursor gases needed to initiate nucleation and early growth
574 (Sellegrì et al., 2019). Therefore, the low condensation sinks are not necessarily required to trigger
575 nucleation and early growth, provided there are high vapor production rates. Because the higher
576 pre-existing particle concentration is an indication of precursor-laden air, but when the
577 condensation sink gets very high, it inhibits aerosol nucleation. Further, at Hyderabad, about half
578 of the NPF events did not display aerosol nucleation (sub-3nm particle formation) with subsequent
579 growth of these particles to larger sizes (>10 nm), perhaps due to lower organic vapor
580 concentrations (Sebastian et al., 2021a). Rose et al. (2017) also reported a high frequency of NPF
581 occurrence for boundary layer (48%) than free troposphere (39%) conditions at Chacaltaya
582 mountain (5240 m amsl), Bolivia. Thus potential CCN formation was higher for NPF events
583 initiated in the boundary layer (67%) than free troposphere (53%). Sellegrì et al. (2019) reviewed
584 the CCN concentrations from NPF events in the boundary layer and high-altitude locations. They
585 revealed that the CCN production is the highest at San Pietro Capofiume, a polluted region of the
586 Po Valley ($7.3 \times 10^3 \text{ cm}^{-3}$) (Laaksonen et al., 2005) as compared to high-altitude sites (Rose et al.,
587 2017; Kerminen et al., 2012). Our findings are similar to these studies showing the highest increase
588 in CCN concentrations in urban locations (HYD, TVM, and DEL) compared to mountain locations
589 (RNC, MUK, and MBL) in India. It is not possible to track the nucleated particle until it becomes
590 a CCN, and they are always mixed with CCN originating from primary sources. This makes it
591 extremely difficult to estimate CCN arising from a given NPF event. In the light of the above
592 discussion, these results offer some insights into potential CCN concentrations originating from
593 NPF.

594

595 **4 Conclusions**

596 In this study, we used at least one year of asynchronous particle number size distribution
597 measurements from six locations in India, consisting of mountain background sites (Ranichauri
598 and Mukteshwar), mountain rural site (Mahabaleshwar), urban sites (Delhi and Hyderabad), and
599 semi-urban coastal site (Thiruvananthapuram). The results from this study provide some insights
600 into the processes influencing particle number size distributions and CCN concentrations in
601 different environments (mountain and urban) of India.



602 We found that the regional NPF was most common in the pre-monsoon (spring) at all the
603 measurement sites, with an exception at TVM where NPF occurred mostly in the late monsoon
604 season (September), which was linked to the inflow of continental air masses that provided a
605 source of low volatile vapors for nucleation. During pre-monsoon, DEL has the highest frequency
606 of NPF occurrence (63.8%), followed by HYD (28.4%) and MBL (15.9%). NPF was the least
607 common during winter at all the sites, particularly at the mountain-background sites (RNC and
608 MUK) without a single NPF event. The high solar insolation (active photochemistry) and the
609 elevated boundary layer (efficient ventilation leading to low pre-existing particles near the surface)
610 explains the most common occurrence of NPF in the pre-monsoon (spring), but this is not a
611 universal NPF frequency pattern in India and elsewhere globally. We found that the J_{NUC} during
612 NPF events tends to increase with an increasing anthropogenic influence, with an order of
613 magnitude higher in urban areas ($0.12 \text{ cm}^{-3} \text{ s}^{-1}$) than mountain sites ($0.06 \text{ cm}^{-3} \text{ s}^{-1}$). We did not find
614 any systematic pattern in GR_{NUC} , with the highest GR_{NUC} at RNC (6.3 nm h^{-1}) and the lowest at
615 TVM (1.1 nm h^{-1}). The observed values of the NPF frequency, J_{NUC} , and GR_{NUC} indicate that the
616 regional NPF events can significantly influence the evolution of particles in the atmosphere. We
617 found that NPF modulates the shape of the particle number size distributions significantly,
618 especially at the mountain background sites (RNC and MUK), which are not directly influenced
619 by the local direct emissions of aerosols (traffic and industries). The number size distribution of
620 particles is higher in pre-monsoon at mountain-background sites, whereas it is higher in winter at
621 urban sites, with the exception of HYD. All sites generally show lower concentrations of particles
622 in monsoon due to the increased removal by wet-scavenging. The histograms of size-segregated
623 particle number concentrations show large variability from one site to another, reflecting the
624 varying contribution of different processes to the total aerosol loading. For instance, the Aitken
625 mode particle concentrations were the highest in pre-monsoon at mountain-background sites (RNC
626 and MUK), whereas they were the highest in winter at urban sites (HYD, TVM, and DEL).
627 Amongst the sites, the lowest measured median total particle number concentration was found in
628 MUK (2658 cm^{-3}) and the highest in DEL (12519 cm^{-3}).

629 We found that the increase in CCN concentrations during an NPF event is higher in urban
630 locations ($4.3 \times 10^3 \text{ cm}^{-3}$ per event and $1.2 \times 10^3 \text{ cm}^{-3}$ per event for 50 nm and 100 nm, respectively)
631 compared to mountain-background sites ($2.7 \times 10^3 \text{ cm}^{-3}$ per event and $1.0 \times 10^3 \text{ cm}^{-3}$ per event for
632 50 nm and 100 nm, respectively). We modified Kerminen and colleague's approach for removing



633 the potential contribution of primary CCN-active particles to give the best possible estimate for
634 the increase in CCN concentrations during a given NPF event. Such analyses should be
635 supplemented by regional model simulations or high spatial resolution measurements of NPF and
636 CCN concentrations.

637

638 **Code availability**

639 Particle number size distributions data was analyzed in IGOR Pro 8.0. Figure 8 was created in
640 IGOR Pro 8.0, while all other figures were created in IDL 8.0.

641

642 **Data availability**

643 Particles data will be made available upon a reasonable request to the corresponding author.

644

645 **Author contribution:**

646 VPK conceived the idea and designed the research. MS and VPK carried out a comprehensive
647 data analysis. MS carried out CCN estimation analysis and interpretation with critical inputs
648 from JRP, VV, and VPK. MS, SKK, AK, and SJ performed particle size distribution
649 measurements and analysis. MS and VPK wrote the first draft, and MS edited with critical inputs
650 from all co-authors.

651

652 **Competing interests**

653 The authors declare that they have no conflict of interest.

654

655 **Acknowledgments**

656 VPK was supported by the Department of Science & Technology (DST)-Science Engineering
657 Research Board (SERB) (ECR/2016/001333) and DST-Climate Change Division Program
658 (Aerosol/89/2017). VKS acknowledges the technical support from Sanjay Rawat for maintaining
659 the Climate Monitoring station at Ranichauri. IITM and HACPL are fully funded by the Ministry
660 of Earth Sciences (MoES), Govt. of India. The data collection at Thiruvananthapuram was carried
661 out under the Aerosol Radiative Forcing over India (ARFI) project of the Indian Space Research
662 Organisation-Geosphere Biosphere Program (ISRO-GBP). RKH, VV, EA and APH acknowledge
663 the Academy of Finland Flagship funding (grant no. 337552). RKH and APH also acknowledge



664 the team of TERI, Mukteshwar and V.P. Sharma for technical support. JRP was supported by the
665 US Department of Energy's Atmospheric System Research, an Office of Science, Office of
666 Biological and Environmental Research Program, under grant DE-SC0019000.

667

668 **References**

669 Kumar, A. V., Hazra, A., Pandithurai, G., Kulkarni, G., Mohan, G. M., Mukherjee, S., Leena, P.
670 P., Patil, R. D., and Prasad, D. S. V. V. D.: Atmospheric ice nucleating particle measurements
671 and parameterization representative for Indian region, *Atmospheric Research*, 253, 105487,
672 <https://doi.org/10.1016/j.atmosres.2021.105487>, 2021.

673 Babu, S. S., Kompalli, S. K., and Moorthy, K. K.: Aerosol number size distributions over a
674 coastal semi urban location: Seasonal changes and ultrafine particle bursts, *Science of The Total*
675 *Environment*, 563–564, 351–365, <http://dx.doi.org/10.1016/j.scitotenv.2016.03.246>, 2016.

676 Bianchi, F., Junninen, H., Bigi, A., Sinclair, V. A., Dada, L., Hoyle, C. R., Zha, Q., Yao, L.,
677 Ahonen, L. R., Bonasoni, P., Buenrostro Mazon, S., Hutterli, M., Laj, P., Lehtipalo, K.,
678 Kangasluoma, J., Kerminen, V. M., Kontkanen, J., Marinoni, A., Mirme, S., Molteni, U., Petäjä,
679 T., Riva, M., Rose, C., Sellegri, K., Yan, C., Worsnop, D. R., Kulmala, M., Baltensperger, U.,
680 and Dommen, J.: Biogenic particles formed in the Himalaya as an important source of free
681 tropospheric aerosols, *Nature Geoscience*, 14, 4–9, [10.1038/s41561-020-00661-5](https://doi.org/10.1038/s41561-020-00661-5), 2021.

682 Bousiotis, D., Brean, J., Pope, F. D., Dall'Osto, M., Querol, X., Alastuey, A., Perez, N., Petäjä,
683 T., Massling, A., Nøjgaard, J. K., Nordstrøm, C., Kouvarakis, G., Vratolis, S., Eleftheriadis, K.,
684 Niemi, J. V., Portin, H., Wiedensohler, A., Weinhold, K., Merkel, M., Tuch, T., and Harrison, R.
685 M.: The effect of meteorological conditions and atmospheric composition in the occurrence and
686 development of new particle formation (NPF) events in Europe, *Atmos. Chem. Phys.*, 21, 3345–
687 3370, [10.5194/acp-21-3345-2021](https://doi.org/10.5194/acp-21-3345-2021), 2021.

688 Census of India: Provisional population totals: rural-urban distribution Volume 2, Issue 1 of
689 Census of India, 2011, India. India: Office of the Registrar General & Census Commissioner,
690 2011.

691 Dal Maso, M., Kulmala, M., Riipinen, I., Wagner, R., Hussein, T., Aalto, P. P., and Lehtinen, K.
692 E. J.: Formation and growth of fresh atmospheric aerosols: eight years of aerosol size distribution
693 data from SMEAR II, Hyytiälä, Finland, *Boreal Env. Res.*, 10, 323–336, 2005.

694 Dunne, E. M., Gordon, H., Kürten, A., Almeida, J., Duplissy, J., Williamson, C., Ortega, I. K.,
695 Pringle, K. J., Adamov, A., Baltensperger, U., Barmet, P., Benduhn, F., Bianchi, F.,
696 Breitenlechner, M., Clarke, A., Curtius, J., Dommen, J., Donahue, N. M., Ehrhart, S., Flagan, R.
697 C., Franchin, A., Guida, R., Hakala, J., Hansel, A., Heinritzi, M., Jokinen, T., Kangasluoma, J.,
698 Kirkby, J., Kulmala, M., Kupc, A., Lawler, M. J., Lehtipalo, K., Makhmutov, V., Mann, G.,
699 Mathot, S., Merikanto, J., Miettinen, P., Nenes, A., Onnela, A., Rap, A., Reddington, C. L. S.,
700 Riccobono, F., Richards, N. A. D., Rissanen, M. P., Rondo, L., Sarnela, N., Schobesberger, S.,
701 Sengupta, K., Simon, M., Sipilä, M., Smith, J. N., Stozkhov, Y., Tomé, A., Tröstl, J., Wagner, P.
702 E., Wimmer, D., Winkler, P. M., Worsnop, D. R., and Carslaw, K. S.: Global atmospheric



- 703 particle formation from CERN CLOUD measurements, *Science*, 354, 1119-1124,
704 10.1126/science.aaf2649, 2016.
- 705 Gani, S., Bhandari, S., Patel, K., Seraj, S., Soni, P., Arub, Z., Habib, G., Hildebrandt Ruiz, L.,
706 and Apte, J. S.: Particle number concentrations and size distribution in a polluted megacity: the
707 Delhi Aerosol Supersite study, *Atmos. Chem. Phys.*, 20, 8533-8549, 10.5194/acp-20-8533-2020,
708 2020.
- 709 Gordon, H., Kirkby, J., Baltensperger, U., Bianchi, F., Breitenlechner, M., Curtius, J., Dias, A.,
710 Dommen, J., Donahue, N. M., Dunne, E. M., Duplissy, J., Ehrhart, S., Flagan, R. C., Frege, C.,
711 Fuchs, C., Hansel, A., Hoyle, C. R., Kulmala, M., Kürten, A., Lehtipalo, K., Makhmutov, V.,
712 Molteni, U., Rissanen, M. P., Stozkhov, Y., Tröstl, J., Tsagkogeorgas, G., Wagner, R.,
713 Williamson, C., Wimmer, D., Winkler, P. M., Yan, C., and Carslaw, K. S.: Causes and
714 importance of new particle formation in the present-day and preindustrial atmospheres, *Journal*
715 *of Geophysical Research: Atmospheres*, 122, 8739-8760, 10.1002/2017jd026844, 2017.
- 716 Grimm, H. and Eatough, D. J.: Aerosol Measurement: The Use of Optical Light Scattering for
717 the Determination of Particulate Size Distribution, and Particulate Mass, Including the Semi-
718 Volatile Fraction, *Journal of the Air & Waste Management Association*, 59, 101-107,
719 10.3155/1047-3289.59.1.101, 2009.
- 720 Guo, S., Hu, M., Zamora, M. L., Peng, J., Shang, D., Zheng, J., Du, Z., Wu, Z., Shao, M., Zeng,
721 L., Molina, M. J., and Zhang, R.: Elucidating severe urban haze formation in China, *Proceedings*
722 *of the National Academy of Sciences*, 111, 17373-17378, 10.1073/pnas.1419604111, 2014.
- 723 Guo, S., Hu, M., Peng, J., Wu, Z., Zamora, M. L., Shang, D., Du, Z., Zheng, J., Fang, X., Tang,
724 R., Wu, Y., Zeng, L., Shuai, S., Zhang, W., Wang, Y., Ji, Y., Li, Y., Zhang, A. L., Wang, W.,
725 Zhang, F., Zhao, J., Gong, X., Wang, C., Molina, M. J., and Zhang, R.: Remarkable nucleation
726 and growth of ultrafine particles from vehicular exhaust, *Proceedings of the National Academy*
727 *of Sciences*, 117, 3427-3432, 10.1073/pnas.1916366117, 2020.
- 728 Hooda, R. K., Kivekäs, N., O'Connor, E. J., Collaud Coen, M., Pietikäinen, J.-P., Vakkari, V.,
729 Backman, J., Henriksson, S. V., Asmi, E., Komppula, M., Korhonen, H., Hyvärinen, A.-P., and
730 Lihavainen, H.: Driving Factors of Aerosol Properties Over the Foothills of Central Himalayas
731 Based on 8.5 Years Continuous Measurements, *Journal of Geophysical Research: Atmospheres*,
732 123, 13,421-413,442, 10.1029/2018jd029744, 2018.
- 733 Hyvärinen, A. P., Lihavainen, H., Komppula, M., Panwar, T. S., Sharma, V. P., Hooda, R. K.,
734 and Viisanen, Y.: Aerosol measurements at the Gual Pahari EUCAARI station: preliminary
735 results from in-situ measurements, *Atmos. Chem. Phys.*, 10, 7241-7252, 10.5194/acp-10-7241-
736 2010, 2010.
- 737 IPCC: Climate Change 2013: The Physical Science Basis. Contribution of Working Group I to
738 the Fifth Assessment Report of the Intergovernmental Panel on Climate Change, Cambridge,
739 United Kingdom and New York, NY, USA, , 1535 pp., 2013.
- 740 Kalivitis, N., Kerminen, V. M., Kouvarakis, G., Stavroulas, I., Bougiatioti, A., Nenes, A.,
741 Manninen, H. E., Petäjä, T., Kulmala, M., and Mihalopoulos, N.: Atmospheric new particle



- 742 formation as a source of CCN in the eastern Mediterranean marine boundary layer, Atmos.
743 Chem. Phys., 15, 9203-9215, 10.5194/acp-15-9203-2015, 2015.
- 744 Kanawade, V. P., Benson, D. R., and Lee, S.-H.: Statistical analysis of 4-year observations of
745 aerosol sizes in a semi-rural continental environment, Atmospheric Environment, 59, 30-38,
746 <http://dx.doi.org/10.1016/j.atmosenv.2012.05.047>, 2012.
- 747 Kanawade, V. P., Sebastian, M., Hooda, R. K., and Hyvärinen, A. P.: Atmospheric new particle
748 formation in India: Current understanding, knowledge gaps and future directions, Atmospheric
749 Environment (under review), 2021.
- 750 Kanawade, V. P., Tripathi, S. N., Bhattu, D., and Shamjad, P. M.: Sub-micron particle number
751 size distributions characteristics at an urban location, Kanpur, in the Indo-Gangetic Plain,
752 Atmospheric Research, 147-148, 121-132, <http://dx.doi.org/10.1016/j.atmosres.2014.05.010>,
753 2014a.
- 754 Kanawade, V. P., Tripathi, S. N., Chakraborty, A., and Yu, H.: Chemical Characterization of
755 Sub-micron Aerosols during New Particle Formation in an Urban Atmosphere, Aerosol and Air
756 Quality Research, 20, 1294-1305, 10.4209/aaqr.2019.04.0196, 2020a.
- 757 Kanawade, V. P., Srivastava, A. K., Ram, K., Asmi, E., Vakkari, V., Soni, V. K., Varaprasad, V.,
758 and Sarangi, C.: What caused severe air pollution episode of November 2016 in New Delhi?,
759 Atmospheric Environment, 222, 117125, <https://doi.org/10.1016/j.atmosenv.2019.117125>,
760 2020b.
- 761 Kanawade, V. P., Tripathi, S. N., Siingh, D., Gautam, A. S., Srivastava, A. K., Kamra, A. K.,
762 Soni, V. K., and Sethi, V.: Observations of new particle formation at two distinct Indian
763 subcontinental urban locations, Atmospheric Environment, 96, 370-379,
764 <http://dx.doi.org/10.1016/j.atmosenv.2014.08.001>, 2014b.
- 765 Kanawade, V. P., Shika, S., Pöhlker, C., Rose, D., Suman, M. N. S., Gadhavi, H., Kumar, A.,
766 Nagendra, S. M. S., Ravikrishna, R., Yu, H., Sahu, L. K., Jayaraman, A., Andreae, M. O.,
767 Pöschl, U., and Gunthe, S. S.: Infrequent occurrence of new particle formation at a semi-rural
768 location, Gadanki, in tropical Southern India, Atmospheric Environment, 94, 264-273,
769 <http://dx.doi.org/10.1016/j.atmosenv.2014.05.046>, 2014c.
- 770 Kerminen, V.-M., Chen, X., Vakkari, V., Petäjä, T., Kulmala, M., and Bianchi, F.: Atmospheric
771 new particle formation and growth: review of field observations, Environmental Research
772 Letters, 13, 103003, 10.1088/1748-9326/aadf3c, 2018.
- 773 Kerminen, V.-M., Paramonov, M., Anttila, T., Riipinen, I., Fountoukis, C., Korhonen, H., Asmi,
774 E., Laakso, L., Lihavainen, H., Swietlicki, E., Svenningsson, B., Asmi, A., Pandis, S. N.,
775 Kulmala, M., and Petäjä, T.: Cloud condensation nuclei production associated with atmospheric
776 nucleation: a synthesis based on existing literature and new results, Atmos. Chem. Phys., 12,
777 12037-12059, 10.5194/acp-12-12037-2012, 2012.



- 778 Kirkby, J., Curtius, J., Almeida, J., Dunne, E., Duplissy, J., Ehrhart, S., Franchin, A., Gagne, S.,
779 Ickes, L., Kurten, A., Kupc, A., Metzger, A., Riccobono, F., Rondo, L., Schobesberger, S.,
780 Tsagkogeorgas, G., Wimmer, D., Amorim, A., Bianchi, F., Breitenlechner, M., David, A.,
781 Dommen, J., Downard, A., Ehn, M., Flagan, R. C., Haider, S., Hansel, A., Hauser, D., Jud, W.,
782 Junninen, H., Kreissl, F., Kvashin, A., Laaksonen, A., Lehtipalo, K., Lima, J., Lovejoy, E. R.,
783 Makhmutov, V., Mathot, S., Mikkila, J., Minginette, P., Mogo, S., Nieminen, T., Onnela, A.,
784 Pereira, P., Petaja, T., Schnitzhofer, R., Seinfeld, J. H., Sipila, M., Stozhkov, Y., Stratmann, F.,
785 Tome, A., Vanhanen, J., Viisanen, Y., Vrtala, A., Wagner, P. E., Walther, H., Weingartner, E.,
786 Wex, H., Winkler, P. M., Carslaw, K. S., Worsnop, D. R., Baltensperger, U., and Kulmala, M.:
787 Role of sulphuric acid, ammonia and galactic cosmic rays in atmospheric aerosol nucleation,
788 *Nature*, 476, 429-433,
789 [http://www.nature.com/nature/journal/v476/n7361/abs/nature10343.html#supplementary-](http://www.nature.com/nature/journal/v476/n7361/abs/nature10343.html#supplementary-information)
790 [information](http://www.nature.com/nature/journal/v476/n7361/abs/nature10343.html#supplementary-information), 2011.
- 791 Kompalli, S. K., Babu, S. S., Udayasoorian, C., and Jayabalakrishnan, R. M.: Role of
792 anthropogenic emissions and meteorology on ultrafine particle bursts over a high altitude site in
793 Western Ghats during pre-monsoon, *Journal of Atmospheric and Solar-Terrestrial Physics*, 179,
794 378-388, <https://doi.org/10.1016/j.jastp.2018.09.001>, 2018.
- 795 Kompalli, S. K., Nair, V. S., Jayachandran, V., Gogoi, M. M., and Babu, S. S.: Particle number
796 size distributions and new particle formation events over the northern Indian Ocean during
797 continental outflow, *Atmospheric Environment*, 238, 117719,
798 <https://doi.org/10.1016/j.atmosenv.2020.117719>, 2020.
- 799 Komppula, M., Lihavainen, H., Hyvärinen, A. P., Kerminen, V.-M., Panwar, T. S., Sharma, V.
800 P., and Viisanen, Y.: Physical properties of aerosol particles at a Himalayan background site in
801 India, *Journal of Geophysical Research: Atmospheres*, 114, n/a-n/a, 10.1029/2008jd011007,
802 2009.
- 803 Kuang, C., McMurry, P. H., and McCormick, A. V.: Determination of cloud condensation nuclei
804 production from measured new particle formation events, *Geophysical Research Letters*, 36, n/a-
805 n/a, 10.1029/2009gl037584, 2009.
- 806 Kulmala, M., Vehkamäki, H., Petäjä, T., Dal Maso, M., Lauri, A., Kerminen, V.-M., Birmili, W.,
807 and McMurry, P. H.: Formation and growth rates of ultrafine atmospheric particles: a review of
808 observations, *Journal of Aerosol Science*, 35, 143-176,
809 <http://dx.doi.org/10.1016/j.jaerosci.2003.10.003>, 2004.
- 810 Kulmala, M., Riipinen, I., Sipilä, M., Manninen, H. E., Petäjä, T., Junninen, H., Maso, M. D.,
811 Mordas, G., Mirme, A., Vana, M., Hirsikko, A., Laakso, L., Harrison, R. M., Hanson, I., Leung,
812 C., Lehtinen, K. E. J., and Kerminen, V.-M.: Toward Direct Measurement of Atmospheric
813 Nucleation, *Science*, 318, 89-92, 10.1126/science.1144124, 2007.
- 814 Kulmala, M., Dada, L., Daellenbach, K. R., Yan, C., Stolzenburg, D., Kontkanen, J., Ezhova, E.,
815 Hakala, S., Tuovinen, S., Kokkonen, T. V., Kurppa, M., Cai, R., Zhou, Y., Yin, R., Baalbaki, R.,
816 Chan, T., Chu, B., Deng, C., Fu, Y., Ge, M., He, H., Heikkinen, L., Junninen, H., Liu, Y., Lu, Y.,
817 Nie, W., Rusanen, A., Vakkari, V., Wang, Y., Yang, G., Yao, L., Zheng, J., Kujansuu, J.,



- 818 Kangasluoma, J., Petäjä, T., Paasonen, P., Järvi, L., Worsnop, D., Ding, A., Liu, Y., Wang, L.,
819 Jiang, J., Bianchi, F., and Kerminen, V.-M.: Is reducing new particle formation a plausible
820 solution to mitigate particulate air pollution in Beijing and other Chinese megacities?, *Faraday*
821 *Discussions*, 226, 334-347, 10.1039/D0FD00078G, 2021.
- 822 Laaksonen, A., Hamed, A., Joutsensaari, J., Hiltunen, L., Cavalli, F., Junkermann, W., Asmi, A.,
823 Fuzzi, S., and Facchini, M. C.: Cloud condensation nucleus production from nucleation events at
824 a highly polluted region, 32, <https://doi.org/10.1029/2004GL022092>, 2005.
- 825 Laj, P., Bigi, A., Rose, C., Andrews, E., Lund Myhre, C., Collaud Coen, M., Lin, Y.,
826 Wiedensohler, A., Schulz, M., Ogren, J. A., Fiebig, M., Gliš, J., Mortier, A., Pandolfi, M.,
827 Petäjä, T., Kim, S. W., Aas, W., Putaud, J. P., Mayol-Bracero, O., Keywood, M., Labrador, L.,
828 Aalto, P., Ahlberg, E., Alados Arboledas, L., Alastuey, A., Andrade, M., Artíñano, B., Ausmeel,
829 S., Arsov, T., Asmi, E., Backman, J., Baltensperger, U., Bastian, S., Bath, O., Beukes, J. P.,
830 Brem, B. T., Bukowiecki, N., Conil, S., Couret, C., Day, D., Dayantolis, W., Degorska, A.,
831 Eleftheriadis, K., Fetfatzis, P., Favez, O., Flentje, H., Gini, M. I., Gregorič, A., Gysel-Beer, M.,
832 Hallar, A. G., Hand, J., Hoffer, A., Hueglin, C., Hooda, R. K., Hyvärinen, A., Kalapov, I.,
833 Kalivitis, N., Kasper-Giebl, A., Kim, J. E., Kouvarakis, G., Kranjc, I., Krejci, R., Kulmala, M.,
834 Labuschagne, C., Lee, H. J., Lihavainen, H., Lin, N. H., Löschau, G., Luoma, K., Marinoni, A.,
835 Martins Dos Santos, S., Meinhardt, F., Merkel, M., Metzger, J. M., Mihalopoulos, N., Nguyen,
836 N. A., Ondracek, J., Pérez, N., Perrone, M. R., Petit, J. E., Picard, D., Pichon, J. M., Pont, V.,
837 Prats, N., Prenni, A., Reisen, F., Romano, S., Sellegri, K., Sharma, S., Schauer, G., Sheridan, P.,
838 Sherman, J. P., Schütze, M., Schwerin, A., Sohmer, R., Sorribas, M., Steinbacher, M., Sun, J.,
839 Titos, G., Toczko, B., Tuch, T., Tulet, P., Tunved, P., Vakkari, V., Velarde, F., Velasquez, P.,
840 Villani, P., Vratolis, S., Wang, S. H., Weinhold, K., Weller, R., Yela, M., Yus-Diez, J., Zdimal,
841 V., Zieger, P., and Zikova, N.: A global analysis of climate-relevant aerosol properties retrieved
842 from the network of Global Atmosphere Watch (GAW) near-surface observatories, *Atmos.*
843 *Meas. Tech.*, 13, 4353-4392, 10.5194/amt-13-4353-2020, 2020.
- 844 Merikanto, J., Spracklen, D. V., Mann, G. W., Pickering, S. J., and Carslaw, K. S.: Impact of
845 nucleation on global CCN, *Atmos. Chem. Phys.*, 9, 8601-8616, 10.5194/acp-9-8601-2009, 2009.
- 846 Moorthy, K. K., Satheesh, S. K., Babu, S. S., and Dutt, C. B. S.: Integrated Campaign for
847 Aerosols, gases and Radiation Budget (ICARB): An overview, *Journal of Earth System Science*,
848 117, 243-262, 10.1007/s12040-008-0029-7, 2008.
- 849 Moorthy, K. K., Sreekanth, V., Prakash Chaubey, J., Gogoi, M. M., Suresh Babu, S., Kumar
850 Kompalli, S., Bagare, S. P., Bhatt, B. C., Gaur, V. K., Prabhu, T. P., and Singh, N. S.: Fine and
851 ultrafine particles at a near-free tropospheric environment over the high-altitude station Hanle in
852 the Trans-Himalaya: New particle formation and size distribution, *Journal of Geophysical*
853 *Research: Atmospheres*, 116, n/a-n/a, 10.1029/2011jd016343, 2011.
- 854 Nair, V. S., Jayachandran, V. N., Kompalli, S. K., Gogoi, M. M., and Babu, S. S.: Cloud
855 condensation nuclei properties of South Asian outflow over the northern Indian Ocean during
856 winter, *Atmos. Chem. Phys.*, 20, 3135-3149, 10.5194/acp-20-3135-2020, 2020.



- 857 Neitola, K., Asmi, E., Komppula, M., Hyvärinen, A. P., Raatikainen, T., Panwar, T. S., Sharma,
858 V. P., and Lihavainen, H.: New particle formation infrequently observed in Himalayan foothills
859 – why?, *Atmos. Chem. Phys.*, 11, 8447-8458, 10.5194/acp-11-8447-2011, 2011.
- 860 Nieminen, T., Kerminen, V.-M., Petäjä, T., Aalto, P. P., Arshinov, M., Asmi, E., Baltensperger,
861 U., Beddows, D. C. S., Beukes, J. P., Collins, D., Ding, A., Harrison, R. M., Henzing, B., Hooda,
862 R., Hu, M., Hörrak, U., Kivekäs, N., Komsaare, K., Krejci, R., Kristensson, A., Laakso, L.,
863 Laaksonen, A., Leaitch, W. R., Lihavainen, H., Mihalopoulos, N., Németh, Z., Nie, W., O'Dowd,
864 C., Salma, I., Sellegri, K., Svenningsson, B., Swietlicki, E., Tunved, P., Ulevicius, V., Vakkari,
865 V., Vana, M., Wiedensohler, A., Wu, Z., Virtanen, A., and Kulmala, M.: Global analysis of
866 continental boundary layer new particle formation based on long-term measurements, *Atmos.*
867 *Chem. Phys.*, 18, 14737-14756, 10.5194/acp-18-14737-2018, 2018.
- 868 Paasonen, P., Asmi, A., Petäjä, T., Kajos, M. K., Äijälä, M., Junninen, H., Holst, T., Abbatt, J. P.
869 D., Arneth, A., Birmili, W., van der Gon, H. D., Hamed, A., Hoffer, A., Laakso, L., Laaksonen,
870 A., Richard Leaitch, W., Plass-Dülmer, C., Pryor, S. C., Räisänen, P., Swietlicki, E.,
871 Wiedensohler, A., Worsnop, D. R., Kerminen, V.-M., and Kulmala, M.: Warming-induced
872 increase in aerosol number concentration likely to moderate climate change, *Nature Geoscience*,
873 6, 438-442, 10.1038/ngeo1800, 2013.
- 874 Pierce, J. R. and Adams, P. J.: Efficiency of cloud condensation nuclei formation from ultrafine
875 particles, *Atmos. Chem. Phys.*, 7, 1367-1379, 10.5194/acp-7-1367-2007, 2007.
- 876 Pierce, J. R., Westervelt, D. M., Atwood, S. A., Barnes, E. A., and Leaitch, W. R.: New-particle
877 formation, growth and climate-relevant particle production in Egbert, Canada: analysis from 1
878 year of size-distribution observations, *Atmos. Chem. Phys.*, 14, 8647-8663, 10.5194/acp-14-
879 8647-2014, 2014.
- 880 Pierce, J. R., Leaitch, W. R., Liggio, J., Westervelt, D. M., Wainwright, C. D., Abbatt, J. P. D.,
881 Ahlm, L., Al-Basheer, W., Cziczo, D. J., Hayden, K. L., Lee, A. K. Y., Li, S. M., Russell, L. M.,
882 Sjostedt, S. J., Strawbridge, K. B., Travis, M., Vlasenko, A., Wentzell, J. J. B., Wiebe, H. A.,
883 Wong, J. P. S., and Macdonald, A. M.: Nucleation and condensational growth to CCN sizes
884 during a sustained pristine biogenic SOA event in a forested mountain valley, *Atmos. Chem.*
885 *Phys.*, 12, 3147-3163, 10.5194/acp-12-3147-2012, 2012.
- 886 Pikridas, M., Riipinen, I., Hildebrandt, L., Kostenidou, E., Manninen, H., Mihalopoulos, N.,
887 Kalivitis, N., Burkhardt, J. F., Stohl, A., Kulmala, M., and Pandis, S. N.: New particle formation
888 at a remote site in the eastern Mediterranean, 117, <https://doi.org/10.1029/2012JD017570>,
889 2012.
- 890 Raatikainen, T., Hyvärinen, A. P., Hatakka, J., Panwar, T. S., Hooda, R. K., Sharma, V. P., and
891 Lihavainen, H.: The effect of boundary layer dynamics on aerosol properties at the Indo-
892 Gangetic plains and at the foothills of the Himalayas, *Atmospheric Environment*, 89, 548-555,
893 <https://doi.org/10.1016/j.atmosenv.2014.02.058>, 2014.
- 894 Ramanathan, V., Crutzen, P. J., Lelieveld, J., Mitra, A. P., Althausen, D., Anderson, J., Andreae,
895 M. O., Cantrell, W., Cass, G. R., Chung, C. E., Clarke, A. D., Coakley, J. A., Collins, W. D.,



- 896 Conant, W. C., Dulac, F., Heintzenberg, J., Heymsfield, A. J., Holben, B., Howell, S., Hudson,
897 J., Jayaraman, A., Kiehl, J. T., Krishnamurti, T. N., Lubin, D., McFarquhar, G., Novakov, T.,
898 Ogren, J. A., Podgorny, I. A., Prather, K., Priestley, K., Prospero, J. M., Quinn, P. K., Rajeev, K.,
899 Rasch, P., Rupert, S., Sadourny, R., Satheesh, S. K., Shaw, G. E., Sheridan, P., and Valero, F. P.
900 J.: Indian Ocean Experiment: An integrated analysis of the climate forcing and effects of the
901 great Indo-Asian haze, 106, 28371-28398, <https://doi.org/10.1029/2001JD900133>, 2001.
- 902 Reddington, C. L., Carslaw, K. S., Spracklen, D. V., Frontoso, M. G., Collins, L., Merikanto, J.,
903 Minikin, A., Hamburger, T., Coe, H., Kulmala, M., Aalto, P., Flentje, H., Plass-Dülmer, C.,
904 Birmili, W., Wiedensohler, A., Wehner, B., Tuch, T., Sonntag, A., O'Dowd, C. D., Jennings, S.
905 G., Dupuy, R., Baltensperger, U., Weingartner, E., Hansson, H. C., Tunved, P., Laj, P., Sellegri,
906 K., Boulon, J., Putaud, J. P., Gruening, C., Swietlicki, E., Roldin, P., Henzing, J. S., Moerman,
907 M., Mihalopoulos, N., Kouvarakis, G., Ždímal, V., Zíková, N., Marinoni, A., Bonasoni, P., and
908 Duchi, R.: Primary versus secondary contributions to particle number concentrations in the
909 European boundary layer, *Atmos. Chem. Phys.*, 11, 12007-12036, 10.5194/acp-11-12007-2011,
910 2011.
- 911 Rodríguez, S., Van Dingenen, R., Putaud, J.-P., Martins-Dos Santos, S., and Roselli, D.:
912 Nucleation and growth of new particles in the rural atmosphere of Northern Italy—relationship
913 to air quality monitoring, *Atmospheric Environment*, 39, 6734-6746,
914 <https://doi.org/10.1016/j.atmosenv.2005.07.036>, 2005.
- 915 Rose, C., Sellegri, K., Moreno, I., Velarde, F., Ramonet, M., Weinhold, K., Krejci, R., Andrade,
916 M., Wiedensohler, A., Ginot, P., and Laj, P.: CCN production by new particle formation in the
917 free troposphere, *Atmos. Chem. Phys.*, 17, 1529-1541, 10.5194/acp-17-1529-2017, 2017.
- 918 Rosenfeld, D., Sherwood, S., Wood, R., and Donner, L.: Climate Effects of Aerosol-Cloud
919 Interactions, *Science*, 343, 379-380, 10.1126/science.1247490, 2014.
- 920 Sarangi, C., Kanawade, V. P., Tripathi, S. N., Thomas, A., and Ganguly, D.: Aerosol-induced
921 intensification of cooling effect of clouds during Indian summer monsoon, *Nature*
922 *Communications*, 9, 3754, 10.1038/s41467-018-06015-5, 2018.
- 923 Schobesberger, S., Franchin, A., Bianchi, F., Rondo, L., Duplissy, J., Kürten, A., Ortega, I. K.,
924 Metzger, A., Schnitzhofer, R., Almeida, J., Amorim, A., Dommen, J., Dunne, E. M., Ehn, M.,
925 Gagné, S., Ickes, L., Junninen, H., Hansel, A., Kerminen, V. M., Kirkby, J., Kupc, A.,
926 Laaksonen, A., Lehtipalo, K., Mathot, S., Onnela, A., Petäjä, T., Riccobono, F., Santos, F. D.,
927 Sipilä, M., Tomé, A., Tsagkogeorgas, G., Viisanen, Y., Wagner, P. E., Wimmer, D., Curtius, J.,
928 Donahue, N. M., Baltensperger, U., Kulmala, M., and Worsnop, D. R.: On the composition of
929 ammonia-sulfuric-acid ion clusters during aerosol particle formation, *Atmos. Chem. Phys.*, 15,
930 55-78, 10.5194/acp-15-55-2015, 2015.
- 931 Sebastian, M., Kanawade, V. P., and Pierce, J. R.: Observation of sub-3nm particles and new
932 particle formation at an urban location in India, *Atmospheric Environment*, 256, 118460,
933 <https://doi.org/10.1016/j.atmosenv.2021.118460>, 2021a.



- 934 Sebastian, M., Kanawade, V., Soni, V., Asmi, E., Westervelt, D., Vakkari, V., Hyvärinen, A. P.,
935 Pierce, J., and Hooda, R.: New Particle Formation and Growth to Climate-Relevant Aerosols at a
936 Background Remote Site in the Western Himalaya, *Journal of Geophysical Research:*
937 *Atmospheres*, 126, 10.1029/2020JD033267, 2021b.
- 938 Sellegri, K., Rose, C., Marinoni, A., Lupi, A., Wiedensohler, A., Andrade, M., Bonasoni, P., and
939 Laj, P.: New Particle Formation: A Review of Ground-Based Observations at Mountain
940 Research Stations, *Atmosphere*, 10, 493, 2019.
- 941 Shika, S., Gadhavi, H., Suman, M. N. S., Ravikrishna, R., and Gunthe, S. S.: Atmospheric
942 aerosol properties at a semi-rural location in southern India: particle size distributions and
943 implications for cloud droplet formation, *SN Applied Sciences*, 2, 1007, 10.1007/s42452-020-
944 2804-2, 2020.
- 945 Sihto, S. L., Mikkilä, J., Vanhanen, J., Ehn, M., Liao, L., Lehtipalo, K., Aalto, P. P., Duplissy, J.,
946 Petäjä, T., Kerminen, V. M., Boy, M., and Kulmala, M.: Seasonal variation of CCN
947 concentrations and aerosol activation properties in boreal forest, *Atmos. Chem. Phys.*, 11, 13269-
948 13285, 10.5194/acp-11-13269-2011, 2011.
- 949 Siingh, D., Gautam, A. S., Buchunde, P., and Kamra, A. K.: Classification of the new particle
950 formation events observed at a tropical site, Pune, India, *Atmospheric Environment*, 190, 10-22,
951 <https://doi.org/10.1016/j.atmosenv.2018.07.025>, 2018.
- 952 Singh, R. P., Dey, S., Tripathi, S. N., Tare, V., and Holben, B.: Variability of aerosol parameters
953 over Kanpur, northern India, 109, <https://doi.org/10.1029/2004JD004966>, 2004.
- 954 Srivastava, A. K., Soni, V. K., Singh, S., Kanawade, V. P., Singh, N., Tiwari, S., and Attri, S. D.:
955 An early South Asian dust storm during March 2012 and its impacts on Indian Himalayan
956 foothills: A case study, *Science of The Total Environment*, 493, 526-534,
957 <https://doi.org/10.1016/j.scitotenv.2014.06.024>, 2014.
- 958 Tare, V., Tripathi, S. N., Chinnam, N., Srivastava, A. K., Dey, S., Manar, M., Kanawade, V. P.,
959 Agarwal, A., Kishore, S., Lal, R. B., and Sharma, M.: Measurements of atmospheric parameters
960 during Indian Space Research Organization Geosphere Biosphere Program Land Campaign II at
961 a typical location in the Ganga Basin: 2. Chemical properties, 111,
962 <https://doi.org/10.1029/2006JD007279>, 2006.
- 963 Thomas, A., Sarangi, C., and Kanawade, V. P.: Recent Increase in Winter Hazy Days over
964 Central India and the Arabian Sea, *Scientific Reports*, 9, 17406, 10.1038/s41598-019-53630-3,
965 2019.
- 966 Tripathi, R. M., Khandekar, R. N., and Mishra, U. C.: Size distribution of atmospheric aerosols
967 in urban sites in India, *Science of The Total Environment*, 77, 237-244,
968 [https://doi.org/10.1016/0048-9697\(88\)90059-9](https://doi.org/10.1016/0048-9697(88)90059-9), 1988.
- 969 Tripathi, S. N., Tare, V., Chinnam, N., Srivastava, A. K., Dey, S., Agarwal, A., Kishore, S., Lal,
970 R. B., Manar, M., Kanawade, V. P., Chauhan, S. S. S., Sharma, M., Reddy, R. R., Gopal, K. R.,



- 971 Narasimhulu, K., Reddy, L. S. S., Gupta, S., and Lal, S.: Measurements of atmospheric
972 parameters during Indian Space Research Organization Geosphere Biosphere Programme Land
973 Campaign II at a typical location in the Ganga basin: 1. Physical and optical properties, 111,
974 <https://doi.org/10.1029/2006JD007278>, 2006.
- 975 Tröstl, J., Herrmann, E., Frege, C., Bianchi, F., Molteni, U., Bukowiecki, N., Hoyle, C. R.,
976 Steinbacher, M., Weingartner, E., Dommen, J., Gysel, M., and Baltensperger, U.: Contribution of
977 new particle formation to the total aerosol concentration at the high-altitude site Jungfraujoch
978 (3580 m asl, Switzerland), *Journal of Geophysical Research: Atmospheres*, 121, 11,692–611,711,
979 10.1002/2015jd024637, 2016.
- 980 Vehkamäki, H. and Riipinen, I.: Thermodynamics and kinetics of atmospheric aerosol particle
981 formation and growth, *Chemical Society Reviews*, 41, 5160–5173, 10.1039/C2CS00002D, 2012.
- 982 Venzac, H., Sellegri, K., Laj, P., Villani, P., Bonasoni, P., Marinoni, A., Cristofanelli, P.,
983 Calzolari, F., Fuzzi, S., Decesari, S., Facchini, M.-C., Vuillermoz, E., and Verza, G. P.: High
984 frequency new particle formation in the Himalayas, *Proceedings of the National Academy of
985 Sciences*, 105, 15666–15671, 10.1073/pnas.0801355105, 2008.
- 986 Westervelt, D. M., Pierce, J. R., and Adams, P. J.: Analysis of feedbacks between nucleation
987 rate, survival probability and cloud condensation nuclei formation, *Atmos. Chem. Phys.*, 14,
988 5577–5597, 10.5194/acp-14-5577-2014, 2014.
- 989 Westervelt, D. M., Pierce, J. R., Riipinen, I., Trivitayanurak, W., Hamed, A., Kulmala, M.,
990 Laaksonen, A., Decesari, S., and Adams, P. J.: Formation and growth of nucleated particles into
991 cloud condensation nuclei: model–measurement comparison, *Atmos. Chem. Phys.*, 13, 7645–
992 7663, 10.5194/acp-13-7645-2013, 2013.
- 993 Wiedensohler, A., Cheng, Y. F., Nowak, A., Wehner, B., Achtert, P., Berghof, M., Birmili, W.,
994 Wu, Z. J., Hu, M., Zhu, T., Takegawa, N., Kita, K., Kondo, Y., Lou, S. R., Hofzumahaus, A.,
995 Holland, F., Wahner, A., Gunthe, S. S., Rose, D., Su, H., and Pöschl, U.: Rapid aerosol particle
996 growth and increase of cloud condensation nucleus activity by secondary aerosol formation and
997 condensation: A case study for regional air pollution in northeastern China, *Journal of
998 Geophysical Research: Atmospheres*, 114, n/a–n/a, 10.1029/2008jd010884, 2009.
- 999 Wiedensohler, A., Birmili, W., Nowak, A., Sonntag, A., Weinhold, K., Merkel, M., Wehner, B.,
1000 Tuch, T., Pfeifer, S., Fiebig, M., Fjåraa, A. M., Asmi, E., Sellegri, K., Depuy, R., Venzac, H.,
1001 Villani, P., Laj, P., Aalto, P., Ogren, J. A., Swietlicki, E., Williams, P., Roldin, P., Quincey, P.,
1002 Hüglin, C., Fierz-Schmidhauser, R., Gysel, M., Weingartner, E., Riccobono, F., Santos, S.,
1003 Grüning, C., Faloon, K., Beddows, D., Harrison, R., Monahan, C., Jennings, S. G., O'Dowd, C.
1004 D., Marinoni, A., Horn, H. G., Keck, L., Jiang, J., Scheckman, J., McMurry, P. H., Deng, Z.,
1005 Zhao, C. S., Moerman, M., Henzing, B., de Leeuw, G., Löschau, G., and Bastian, S.: Mobility
1006 particle size spectrometers: harmonization of technical standards and data structure to facilitate
1007 high quality long-term observations of atmospheric particle number size distributions, *Atmos.
1008 Meas. Tech.*, 5, 657–685, 10.5194/amt-5-657-2012, 2012.



- 1009 Xiao, M., Hoyle, C. R., Dada, L., Stolzenburg, D., Kürten, A., Wang, M., Lamkaddam, H.,
1010 Garmash, O., Mentler, B., Molteni, U., Baccharini, A., Simon, M., He, X. C., Lehtipalo, K.,
1011 Ahonen, L. R., Baalbaki, R., Bauer, P. S., Beck, L., Bell, D., Bianchi, F., Brilke, S., Chen, D.,
1012 Chiu, R., Dias, A., Duplissy, J., Finkenzeller, H., Gordon, H., Hofbauer, V., Kim, C., Koenig, T.
1013 K., Lampilahti, J., Lee, C. P., Li, Z., Mai, H., Makhmutov, V., Manninen, H. E., Marten, R.,
1014 Mathot, S., Mauldin, R. L., Nie, W., Onnela, A., Partoll, E., Petäjä, T., Pfeifer, J., Pospisilova,
1015 V., Quéléver, L. L. J., Rissanen, M., Schobesberger, S., Schuchmann, S., Stozhkov, Y., Tauber,
1016 C., Tham, Y. J., Tomé, A., Vazquez-Pufleau, M., Wagner, A. C., Wanger, R., Wang, Y., Weitz,
1017 L., Wimmer, D., Wu, Y., Yan, C., Ye, P., Ye, Q., Zha, Q., Zhou, X., Amorim, A., Carslaw, K.,
1018 Curtius, J., Hansel, A., Volkamer, R., Winkler, P. M., Flagan, R. C., Kulmala, M., Worsnop, D.
1019 R., Kirkby, J., Donahue, N. M., Baltensperger, U., El Haddad, I., and Dommen, J.: The driving
1020 factors of new particle formation and growth in the polluted boundary layer, *Atmos. Chem. Phys.*
1021 *Discuss.*, 2021, 1-28, 10.5194/acp-2020-1323, 2021.
- 1022 Yu, F., Luo, G., Nair, A. A., Schwab, J. J., Sherman, J. P., and Zhang, Y.: Wintertime new
1023 particle formation and its contribution to cloud condensation nuclei in the Northeastern United
1024 States, *Atmos. Chem. Phys.*, 20, 2591-2601, 10.5194/acp-20-2591-2020, 2020.
- 1025 Yu, H., Ren, L., and Kanawade, V. P.: New Particle Formation and Growth Mechanisms in
1026 Highly Polluted Environments, *Current Pollution Reports*, 3, 245-253, 10.1007/s40726-017-
1027 0067-3, 2017.
- 1028 Zhang, R., Khalizov, A., Wang, L., Hu, M., and Xu, W.: Nucleation and Growth of
1029 Nanoparticles in the Atmosphere, *Chemical Reviews*, 112, 1957-2011, 10.1021/cr2001756,
1030 2012.
- 1031